arXiv:1407.7879v1 [astro-ph.EP] 29 Jul 2014

Hot Jupiters and Cool Stars

Eva Villaver

Universidad Autónoma de Madrid, Department of Theoretical Physics, Módulo 8, 28049 Madrid, Spain

eva.villaver@uam.es

Mario Livio

Space Telescope Science Institute, 3700 San Martin Drive, Baltimore, MD 21218, USA

Alexander J. Mustill

Universidad Autónoma de Madrid, Department of Theoretical Physics, Módulo 8, 28049 Madrid, Spain

Department of Astronomy and Theoretical Physics, Lund University, Box 43, SE-221 00 Lund, Sweden

and

Lionel Siess

Institut d'Astronomie et d'Astrophysique, Université Libre de Bruxelles, B-1050 Bruxelles, Belgium

ABSTRACT

Close-in planets are in jeopardy as their host stars evolve off the main sequence to the subgiant and red giant phases. In this paper, we explore the influences of the stellar mass (in the range 1.5–2$M_{\odot}$), mass-loss prescription, planet mass (from Neptune up to 10 Jupiter masses), and eccentricity, on the orbital evolution of planets as their parent stars evolve to become subgiants and Red Giants. We find that planet engulfment during the Red Giant Branch is not very sensitive to the stellar mass or mass-loss rates adopted in the calculations, but quite sensitive to the planetary mass. The range of initial separations for planet engulfment increases with decreasing mass-loss rates or stellar mass and increasing planetary masses. Regarding the planet's orbital eccentricity, we find that as the star evolves into the red giant phase, stellar tides start to dominate over planetary tides. As a consequence, a transient population of moderately eccentric close-in

Jovian planets is created, that otherwise would have been expected to be absent from main sequence stars. We find that very eccentric and distant planets do not experience much eccentricity decay, and that planet engulfment is primarily determined by the pericenter distance and the maximum stellar radius.

Subject headings: Planetary systems; stars: evolution; stars: fundamental parameters; stars: general

1. INTRODUCTION

Planets orbiting evolved stars offer opportunities to explore a wide range of physical processes that are not applicable to main sequence hosts. These processes include orbital evolution under the influence of tides and mass-loss, planetary ejection or evaporation, instabilities, and the evolution of binary systems (e.g., Villaver & Livio 2007, 2009; Duncan & Lissauer 1998; Debes & Sigurdsson 2002; Kunitomo et al. 2011; Bear & Soker 2011; Mustill & Villaver 2012; Nordhaus et al. 2010; Nordhaus & Spiegel 2013; Moeckel & Veras 2012; Kratter & Perets 2012; Veras et al. 2011, 2013).

Observations show that there is a deficiency of close-in planets around evolved stars (Johnson et al. 2007; Lovis & Mayor 2007; Sato et al. 2007), compared to their main sequence counterparts, even though the two samples have been observed using the same radial velocity technique (e.g., Johnson et al. 2007; Sato et al. 2008; Wright et al. 2009; Niedzielski et al. 2009). The masses of these evolved stars derived from stellar model fitting are typically higher than those of main-sequence planet hosts. At the same time, evolved stars that are hosting planets do not seem to show differences in their Galactic velocity distribution from F5-G5 main sequence stars (Schlaufman & Winn 2013; Maldonado et al. 2013) suggesting that the masses of the evolved stars are similar to main-sequence planet hosts.

Two different mechanisms (not necessarily mutually exclusive) have been proposed to explain the distribution of planetary orbits around evolved stars. One is based on the dispersal timescale of protoplanetary disks, and is directly related to the stellar mass (e.g., Currie 2009), and the other relies on tidal interaction and orbital decay (e.g., Villaver & Livio 2009). The former mechanism requires the masses of the evolved stars to be higher than those of the main sequence hosts. Whether or not this condition is consistent with observations has recently been the topic of some debate (Lloyd 2013; Schlaufman & Winn 2013; Johnson et al. 2013).

The fact remains, however, that both stellar evolution and tidal interaction still in-

volve considerable uncertainties. For instance, the prescription used for mass loss affects the orbital evolution both directly as winds carry away angular momentum, and through its effects on the stellar radius (and thereby on tidal interaction). The ratio of planet mass to stellar mass also strongly affects tides. Previous studies of the orbital evolution of planetary systems around RGB stars did not investigate either the effects of the adopted mass-loss prescription or the planet's eccentricity evolution (e.g., Villaver & Livio 2009; Kunitomo et al. 2011); focused on large orbital distances (Veras et al. 2011); or on the outcome of the orbital evolution in a later stage, the Asymptotic Giant Branch phase and its relevance for the detection of systems during the white dwarf phase (Nordhaus et al. 2010; Nordhaus & Spiegel 2013; Mustill & Villaver 2012). Although a range of stellar masses has been considered by Kunitomo et al. (2011) their tidal evolution calculation was greatly simplified because of the unavailability of the the internal stellar structure needed for the calculation in their models.

In the present work, we present detailed, self consistent, stellar models coupled with orbital evolution. Our computational grid encompasses the evolution from the main sequence, and up to the onset of Helium burning in the stellar core. We have selected a range of stellar masses from 1.5 $M_{\odot}$ to 2 $M_{\odot}$, in steps of 0.1 $M_{\odot}$, and for each stellar mass we have computed the evolution of the star with 3 different prescriptions for the mass-loss. For each star, we have calculated the orbital evolution with planetary masses corresponding that of Neptune, and to 1, 2, 5, and 10 Jupiter masses. We have also considered the planet's eccentricity evolution. Our goal is to characterize and quantify the effects of mass-loss, stellar mass (in an interesting range), planetary mass and eccentricity on planet survival along the Red Giant Branch (RGB) phase.

2. THE CALCULATIONS

We follow the same procedure as in Villaver & Livio (2009) (from now on VL09) and Mustill & Villaver (2012) to determine the planet orbital and eccentricity evolution as the star evolves off the Main Sequence(MS) and up the RGB. We take into account the changes in the mass of the star, the gravitational and frictional drag, and the tidal force. We have not evaluated in this paper either the accretion onto, or the ablation of matter from, the surface of the planet. Based on the estimates provided by the prescription given in VL09 we find that the effect of mass-loss from the star dominates over those processes, even when small RGB mass-loss rates are considered.

We use three different prescriptions for the mass-loss in this paper; two that follow a Reimers' law valid for Red Giants (Reimers 1975) and use values of η_R (the Reimers

parameter) of 0.2 and 0.5 in the formula,

$$\dot{M}_{\rm R} = 4 \times 10^{-13}\, \eta_R \frac{L_\star R_\star}{M_\star} \quad [M_\odot \ {\rm yr}^{-1}] \ , \tag{1}$$

and a third one based on the new semiempirical relation provided by Schröder & Cuntz (2005)

$$\dot{M}_{\rm Sc} = \eta \frac{L_\star R_\star}{M_\star} \left(\frac{Teff}{4000K}\right)^{3.5} \left(1 + \frac{g_\odot}{4300 g_\star}\right) \quad [M_\odot \ {\rm yr}^{-1}] \ , \tag{2}$$

where $L_\star$, $R_\star$, $g_\star$ and $M_\star$ are the stellar luminosity, radius, surface gravity, and mass respectively (in solar units) and the factor $\eta = 8 \times 10^{-14}$ has been obtained by fitting the theoretical relation to observations of globular clusters with different metallicities; $g_\odot$ is the Sun's surface gravity. Thus, the rate of change of the stellar mass is simply given by $\dot{M}_\star = -\dot{M}_{\rm R}$, or $\dot{M}_\star = -\dot{M}_{\rm Sc}$. The stellar evolution calculations have been self-consistently carried out using these 3 mass-loss prescriptions (see §2.1 for details).

We consider that a planet of mass M_p and radius R_p is orbiting with a velocity, v a star of mass $M_\star$. Conservation of angular momentum gives the equation for the rate of change in the semimajor axis of the planet assuming that the time-scale for mass loss is much greater than the orbital time-scale (see, e.g., Alexander et al. 1976; Livio & Soker 1984; Villaver & Livio 2009; Mustill & Villaver 2012),

$$\left(\frac{\dot{a}}{a}\right) = -\frac{\dot{M}_\star}{M_\star + M_p} - \frac{2}{M_p v}\left[F_f + F_g\right] - \left(\frac{\dot{a}}{a}\right)_t \ , \tag{3}$$

where $(\dot{a}/a)_t$ is the rate of orbital decay due to the tidal interaction and F_f and F_g are respectively the frictional and gravitational drag forces which have been computed with the prescription given in VL09. The frictional force is expressed in the form (e.g., Rosenhead 1963)

$$F_f = \frac{1}{2} C_d \rho v^2 \pi R_p^2 \ , \tag{4}$$

where $C_d \simeq 0.9$ is the dimensionless drag coefficient for a sphere, and the gravitational drag force, F_g has the functional form given by (e.g., Ostriker 1999, and references therein)

$$F_g = 4\pi \frac{(G M_p)^2}{c_s^2} \rho I \ , \tag{5}$$

where for I we used the value $I \simeq 0.5$ which is appropriate for the range of Mach numbers for this problem.

We consider tides acting on both the planet and the star. For the planetary tides, we use the formalism of Dobbs-Dixon et al. (2004) with a fixed tidal dissipation efficiency

parameter $Q'_{\rm pl}$, while for the stellar tides, we adopt the formalism of Zahn (1977), in which tidal energy is dissipated by turbulent motions in the star's convective envelope. In fact, in giant stars, which have massive convective envelopes, the most efficient mechanism to produce tidal friction is turbulent viscosity (e.g., Zahn 1966, 1977, 1989). For the angular momentum loss associated to the tidal term $(\dot{a}/a)_t$, the dissipation timescale is determined by the effective eddy viscosity, with eddy velocities and length scales given approximately by standard mixing length theory if convection transports most of the energy flux (Zahn 1989; Verbunt & Phinney 1995; Rasio et al. 1996). The stellar tidal term is given by

$$\left(\frac{\dot{a}}{a}\right)_t = \frac{1}{9\tau_d}\frac{M_{\rm env}}{M_\star}q(1+q)\left(\frac{R_\star}{a}\right)^8 \times \left[2f_2 + e^2\left(\frac{7}{8}f_1 - 10f_2 + \frac{441}{8}f_3\right)\right], \tag{6}$$

and the planet eccentricity decays as

$$\frac{\dot{e}}{e} = -\frac{1}{36\tau_d}\frac{M_{\rm env}}{M_\star}q(1+q)\left(\frac{R_\star}{a}\right)^8 \times \left[\frac{5}{4}f_1 - 2f_2 + \frac{147}{4}f_3\right], \tag{7}$$

with $M_{\rm env}$ and $R_{\rm env}$ being the mass and radial extent of the convective envelope respectively, $q = M_p/M_\star$, and τ_d is the eddy turnover timescale in the stellar envelope

$$\tau_d = \left[\frac{M_{\rm env}\left(R_\star - R_{\rm env}\right)^2}{3L_\star}\right]^{1/3}. \tag{8}$$

The frequency components f_i are given by

$$f_i = f' \min\left[1, \left(\frac{2\pi}{in c_{\rm F}\tau_d}\right)^\gamma\right], \tag{9}$$

where in, with n the mean motion, are the individual frequency components. As in VL09 and Mustill & Villaver (2012) we have used $c_{\rm F} = 1$, $f' = 9/2$ and a value of $\gamma = 2$ which is consistent with the results obtained from numerical calculations (e.g., Zahn 1977; Goldreich & Nicholson 1977; Penev et al. 2007).

In this study, we have made a particular choice, turbulent convection, for the dissipation of the equilibrium tide. So under our assumption, if the star does not have a convective envelope, there is no tide. For stars with radiative envelopes, the use of the Q formalism circumvents this problem by parameterizing the strength of the tidal forces into a variable $Q'_\star$. When the $Q'_\star$ parameter is calibrated using MS stars has values in the $10^5 - 10^{10}$ range (e.g., Jackson et al. 2008a, 2009; Penev & Sasselov 2011). However, for giant stars, a much smaller $Q'_\star \approx 10^2 - 10^3$ is found by Nordhaus et al. (2010) to be equivalent to the Zahn (1977) formalism. Note that since giant stars have deep convective zones the most appropiate mechanism to describe the equilibrium tide is the one adopted here (e.g., Ogilvie

2014). Thus it is inappropriate to apply the Q formalism using the MS calibration for our stars and will anyhow result on much weaker tides than assumed. We have neglected other tidal mechanisms such as dynamical tides (e.g., Witte & Savonije 2002), which although may be important for massive stars during the MS they are mostly irrelevant for the computations for convective stars presented here.

Only during the MS phase we might have a non-convective star. Thus for stars without a convection zone and just in order to avoid numerical round-off errors we set the convective time-scale to an arbitrarily large value (10^9 years). Note that during the MS we are only studying the eccentricity evolution for which only the planetary tides are important.

For eccentric orbits we have also implemented a planetary tide using the standard Q model (e.g., Matsumura et al. 2010). The planet's semi-major axis, eccentricity and spin rate then evolve according to,

$$\frac{\dot{e}}{e} = -\frac{81n}{2Q'_{\rm p}}\frac{1}{q}\left(\frac{R_{\rm p}}{a}\right)^5 \times \left[g_3\left(1-e^2\right)^{-13/2} - \frac{11g_4\left(1-e^2\right)^{-5}\Omega_{\rm p}}{18n}\right] \quad (10)$$

$$\frac{\dot{a}}{a} = \frac{2e\dot{e}}{1-e^2} - \frac{9}{Q'_{\rm p}}\frac{1}{q}\left(\frac{R_{\rm p}}{a}\right)^5 \times \left[g_2\left(1-e^2\right)^{-13/2} n - g_5\left(1-e^2\right)^{-5}\Omega_{\rm p}\right] \quad (11)$$

$$\dot{\Omega}_{\rm p} = \frac{9n^2}{2\alpha_{\rm p}Q'_{\rm p}}\frac{1}{q}\left(\frac{R_{\rm p}}{a}\right)^3 \times \left[g_2\left(1-e^2\right)^{-6} - g_5\left(1-e^2\right)^{-4.5}\frac{\Omega_{\rm p}}{n}\right]. \quad (12)$$

where $R_{\rm p}$ is the planet's radius. The eccentricity functions g_i are given by

$$g_2 = 1 + \frac{15}{2}e^2 + \frac{45}{8}e^4 + \frac{5}{16}e^6 \quad (13)$$

$$g_3 = 1 + \frac{15}{4}e^2 + \frac{15}{8}e^4 + \frac{5}{64}e^6 \quad (14)$$

$$g_4 = 1 + \frac{3}{2}e^2 + \frac{1}{8}e^4 \quad (15)$$

$$g_5 = 1 + 3e^2 + \frac{3}{8}e^4. \quad (16)$$

We note that, while the planet tidal equations are valid for arbitrary planet eccentricities, the stellar tidal equations are based on the lowest-order expansion of the equations and are not strictly valid when the planetary eccentricity is high (note that in Zahn (1989) the $\dot{a}$ equation is valid for any eccentricity but he uses the weak approximation). The reason for this lies in the stellar tidal model; the different Fourier components have different frequency dependencies, and as the eccentricity rises, higher-frequency Fourier components come into play. Nevertheless, for this exploratory study, we used the truncated equations even for highly eccentric planets, deferring a full expansion of the tidal forces to future work. It

is important to keep in mind as well that, as discussed in Mustill & Villaver (2012), the parameters in the tidal equations are poorly known, and consequently the tidal forces may be stronger or weaker than assumed here.

The main uncertainty in the tidal model used comes from the need to reduce the effective viscosity when the tidal period is short compared to the typical convective timescale (e.g., Ogilvie 2014). This is taken into account by variations in the power index γ in Eq. 9. As γ increases the tidal disipation becomes less efficient but only when the planet's orbital period is shorter than the eddy turnover timescale in the stellar envelope. We have chosen a $\gamma = 2$ in Eq. 9 consistent with the results of Ogilvie & Lesur (2012), earlier results of Penev et al. (2007) suggested a $\gamma = 1$.

The tidal model is only sensitive to the assumed value of γ for small orbital distances when the stellar radius is small (e.g., Kunitomo et al. 2011). Thus variations in the power index will not lead to any significant changes in the final outcome of our planets since we are dealing with stars that reach a large radius at the tip of the RGB. If the planet has such a short orbital period to be sensitive to the adopted γ then it would be engulfed very early by the expansion of the star.

Measurements of the spin rates of giants provide average values of $vsini \leq 2\,\mathrm{km\,s^{-1}}$(e.g., de Medeiros et al. 1996; Massarotti et al. 2008), with rapid rotators found only in a few percent (1-2 %) of giant stars (Carlberg et al. 2011). These observations justify our assumption of using non-rotating stars for the calculation of the tidal forces. Planet spin rates were allowed with values between 10 and 1000 radians per year.

A proper calculation of the stellar tides requires knowledge of the stellar structure (i.e. $M_{\rm env}$ and $R_{\rm env}$). Note that some calculations in the literature, do not have this information and as result they rely on simplifications such as the assumption that $M_{\rm env} = M_\star$ and $R_{\rm env} = 0$ for the evaluation of the effects of tidal dissipation on the planet's orbital evolution.

2.1. The Stellar Models

The stellar evolution models were calculated with the STAREVOL code (Siess 2006). We have computed a small grid of non-rotating models with initial masses in the range 1.5 and 2 $M_\odot$ in mass steps of 0.1 $M_\odot$. Based on the observations by Maldonado et al. (2013) we have chosen a stellar metallicity that fullfils two requirements: i) it is consistent with the observed metallicity of planet-hosting giant stars with stellar masses $M_\star > 1.5$ $M_\odot$; and ii) it agrees with the observed metallicities of subgiant stars with planets detected. The initial metallicity is thus set to [Fe/H]=0.19 with a composition scaled solar according to Grevesse et al. (1996).

We do not consider any "extra-mixing processes" such as overshooting or thermohaline mixing and use the Schwarzschild criterion to define the convective boundaries. We adopt $\alpha_{\rm MLT} = 1.75$ for the mixing length parameter which value was determined from solar fitting models. As described above, we considered three representative mass-loss rate prescriptions (see Eqs. 1 and 2).

The extent of the RGB on the HR diagram is very sensitive to the stellar mass for values around the transition mass that marks the border between degenerate and non-degenerate cores. We use here RGB models with masses lower than 2.0 $M_{\odot}$ because they develop electron degenerate He cores after the end of central H-burning for Solar metallicity. These stars have an extended and luminous RGB phase prior to Helium ignition and therefore represent the most interesting arena for the problem analyzed in this paper. The maximum stellar luminosity at the tip of the RGB is reached for stars with degenerate cores and it translates into a maximum stellar radius reached during the RGB. Higher mass stars can ignite helium quietly, terminating the ascent up the RGB before electron degeneracy becomes appreciable in the core, and they reach smaller radii than stars with degenerate cores. Note, however, that the precise value of the transition mass between low and intermediate mass stars depends on the initial chemical composition (e.g., Sweigart et al. 1989, 1990). Decreasing the initial Helium abundance or increasing the heavy element abundances leads to higher transition stellar masses. Thus for stars born in higher metallicity environments, we have larger initial masses marking the transition between degenerate and non-degenerate He cores.

We summarize in Table 1 some of the properties of our stellar models. Column (1) gives the initial mass; column (2) the mass-loss prescription used where Sc refers to the Schröder & Cuntz (2005) model and $\eta_R = 0.5 + OS$ is a model with overshooting; column (3) gives the stellar mass at the time of the deepest extent of the convective envelope during the first Dredge-up (1DUP); columns (4), (5), and (6) give the stellar mass, radius and luminosity at the tip of the RGB respectively; column (7) provides the mass of the Hydrogen depleted core; column (8) the mass-loss rate at the tip of the RGB, and column (9) gives the duration of the RGB phase between the time of the 1DUP and the RGB tip. Finally column (10) gives the minimum initial orbital distance to avoid engulfment at the tip of the RGB calculated for a planet with the mass of Jupiter.

3. RESULTS

As hydrogen becomes exhausted at the center of the star, core contraction accelerates and the star leaves the main sequence on the HR diagram. The major energy production source shifts to a thick shell outside the core where shell ignition drives envelope expansion

and causes the stellar radius to increase (e.g., Iben 1967). Shortly after the star reaches the base of the RGB, convection expands inward from the surface and the first dredge-up takes place.

The planet's orbital evolution was computed by solving the system of Eqs. 3 – 16 coupled with the stellar structure evolution. We did so for each of the six stellar masses and three mass-loss prescriptions considered (a total of 18 stellar models) and we used five planetary masses. For each one of these 90 models we then calculated the orbital evolution by varying the initial orbital separation between 0.1 and 3.5 AU using steps of 0.01 AU. Every integration timestep included an update of the stellar structure (fundamental for an accurate calculation of the stellar tide) and of the variable mass-loss rates. We have introduced also a constraint in the orbital integration timestep so that it was never larger than the timestep at which a significant change in the stellar structure took place.

We first consider circular orbits ($e = 0$) in Eqs. 6 to 16 to investigate the effects of changing the stellar models. For the systems considered in this paper, tidal dissipation in the star dominates (see e.g. Matsumura et al. 2010), and thus we justify circular orbits (for now) on the basis of the fact that both the eccentricity and the semi-major axis damp on similar time-scales (Mustill & Villaver 2012). Note as well that the initial value of the eccentricity has little effect on the orbital decay rate (e.g., Jackson et al. 2008a,b).

We first focus on estimating variations induced by varying parameters such as mass-loss, stellar mass or planet mass, and we defer the discussion of the eccentric orbits to §3.4.

The combined effects of tidally induced orbital decay and mass-loss induced orbital expansion modifies the orbit of the planets in a simple way. If the initial planet separation is within a certain range of distances from the star, the planet will experience an orbital decay caused by the tidal interaction. This ends up with the planet plunging into the stellar envelope. If, on the other hand, the initial orbit is beyond a certain radius, the planet avoids engulfment.

Fig. 1 shows Jupiter mass planet's orbits during ≈ 0.06 Gyr along the RGB phase for a range of initial orbital distances and a particular stellar model (1.5 $M_{\odot}$ with the Schröder & Cuntz 2005 mass-loss prescription). A few features in Fig. 1 are worth noting. First, marked with a solid black line is the initial orbital distance beyond which the planet avoids falling into the stellar envelope during the RGB phase. Every initial separation below the solid black line terminates with the planet being engulfed.

What happens to those planets that enter the envelope largely depends on the ratio of the planet's mass to the envelope mass. Many will end up merging with the stellar core, given the fast decay of the orbit induced by the strong drag forces (Nordhaus & Blackman 2006;

Siess & Livio 1999a,b). Rough estimates of planet survival inside stellar envelopes provide minimum masses of the order of 10-15 Jovian masses (again, depending also on the envelope's mass; Villaver & Livio 2007; Nordhaus et al. 2010). An analysis of the possible progenitors of the planets found orbiting the horizontal branch star KIC 05807616 (Charpinet et al. 2011) also concludes that the surviving planets likely had a mass of a few Jupiter masses (Passy et al. 2012). Note that for survival to occur, a planet must be able to supply enough of its orbital energy to the stellar envelope to unbind the latter before the planet spirals into the disruption region or the stellar core. Unfortunately, the efficiency of the process of unbinding (commonly parameterized with α_{CE}, e.g. Livio & Soker 1988) is rather uncertain. Given that the largest planet mass we are considering is 10 M_J, our working hypothesis in this paper is that whenever the planet gets inside the stellar envelope it would be destroyed. We defer further discussion of planetary systems entering stellar envelopes for a forthcoming study.

The second important feature of the planet's orbital evolution that is important to mention is the range of initial orbital distances that experience tidal decay but that still manage to avoid entering the surface of the star. This range of orbits lies in Fig. 1 close to the solid line. The dot-dashed black line shows a typical example of an orbit dominated by mass-loss. The orbital decay can be substantial for initial orbits close to the critical limit (marked by the solid black line) with the planet ending up in a significantly tighter orbit than the initial one. Planets that start at orbital distances sligthly larger than marked by the solid line, still experience the consequences of tidal forces, but once helium burning is ignited in the core, the star contracts and the interaction stops. Planets in this initial range do not reach the stellar envelope but end up at smaller separations.

Beyond the dot-dashed line in Fig. 1 the orbits increase due to mass-loss from the system.

3.1. The Effects of RGB Mass-Loss

Eq. 3 clearly suggests that the critical orbital distance for engulfment, and the distance beyond which the separation is expected to increase are sensitively dependent on the mass-loss prescription adopted in the calculations (for an analytical treatment of the problem see Adams & Bloch 2013). The purpose of our self-consistent calculation, with models under different mass-loss prescriptions, is to quantify the influence of this relatively poorly constrained parameter on planet survival during the RGB evolution.

Along the RGB the models under different mass-loss prescriptions show significant dif-

ferences associated entirely with the way these stars are losing mass (see Table 1). The mass-loss rate during the RGB is relatively smooth (see Eqs 1 and 2) and never reaches high values (see Fig. 2). The largest and smallest mass-loss rates are attained for the $\eta_R = 0.5$, and $\eta_R = 0.2$ prescriptions respectively, with the Schröder & Cuntz (2005) model having mass-loss rates in between these two values. In Fig. 2 we have plotted the evolution of the mass-loss under the 3 prescriptions used for the 1.5 $M_\odot$ model. In Fig. 3 we show the stellar mass reached at the tip of the RGB versus the stellar MS mass.

We tried to capture the main differences in the planet survival limit among the models in Fig. 4 where we show for the 1.5 $M_\odot$ star the different evolution of the stellar radius for the three mass-loss prescriptions considered (in red, blue and green for $\eta_R = 0.2$, $\eta_R = 0.5$, and Schröder & Cuntz 2005 respectively) and how this leads to different orbital evolution for a Jupiter mass planet. The evolution of the maximum initial orbit that enters the stellar envelope is shown for each the mass-loss prescriptions considered. For the Schröder & Cuntz (2005) model (in green) we have plotted as well as a set of initial orbits representative of the different possible outcomes.

The evolutionary sequences are indistinguishable in terms of the stellar radius during the subgiant phase when mass-loss is negligible and the models do not show significant differences (but not when the star starts the ascent onto the RGB). Typical values of the radius at the RGB tip are given for the different stellar models in Table 1.

Mass-loss influences planet survival due to three combined effects: (i) it modifies the stellar radius, (ii) it changes the orbital angular momentum loss efficiency, and (iii) it changes the stellar mass and thus its evolutionary timescales. When comparing identical mass-loss prescriptions, if the mass-loss rate is higher (the $\eta_R = 0.5$ case), the pressure on the core is reduced and off-center helium ignition is delayed. The star reaches smaller radii and spends more time on the RGB. Lower mass-loss rates under the same prescription for a given stellar and planet mass, lead to more distant planets plunging into the stellar surface due to the combined effects mentioned above. This is why using the lowest mass-loss rate simulation, the one using Reimers with $\eta_R = 0.2$, we obtain the largest critical distance for engulfment (see Fig. 4). The impact of mass-loss on the stellar properties, however, is a highly non-linear process that depends on how fast the mass-loss accelerates along the RGB. Note the longer resulting RGB evolutionary timescales obtained for the Schröder & Cuntz (2005) model.

The minimum initial orbital distances that a Jupiter mass planet has to have in order to avoid engulfment are given in the last column of Table 1, for the different stellar models used in the calculation. We obtain critical values for the engulfment radius that are always in the upper envelope of those plotted by Kunitomo et al. (2011) in their figures (for stars M$\geq$ 1.8–2$M_\odot$) but are consistent with those obtained for stars M$\in$ [1.5–1.7] $M_\odot$. Given the

simplification for the tidal forces these authors made in their paper we have tried to compute the a_{crit} obtained from their Eq. 7 to see if this could be the cause of the difference. We obtain using this equation unrealistic critical distances using the numbers provided by our stellar models, the a_{crit} we get under their prescription are very different from the values we obtain with our full calculation. Generally, we find it hard to reproduce the numbers plotted in their graphs.

In their computation for the critical distance Kunitomo et al. (2011) argued that the differences between the critical distance for engulfment obtained by Villaver & Livio (2009) and their models was due to the inclusion of overshooting. In order to check this assertion we have computed 3 models (for $M_\star$=1.5, 1.7 and 1.9 $M_\odot$) using $\eta_R = 0.5$ and including overshooting with the same prescription by Kunitomo et al. (2011) ($\eta_R = 0.5 + OS$ in Table. 1) . The critical distances we obtain are similar to the ones obtained in our models without overshooting $\eta_R = 0.5$. We believe that the major differences between ours and the Kunitomo et al. (2011) models are a consequence of having transition between degenerate and non-degenerate cores at lower stellar masses, and that cannot be attributable only to the inclusion of overshooting in the models.

3.2. Stellar Mass

The stellar mass explicitly enters into the orbital evolution calculations, affecting the relative strength of the different terms in the angular momentum conservation equations (with the exception of the drag and frictional forces). Furthermore, the mass of the star affects both the evolution of the radius and the maximum radius reached at the end of the RGB. We have quantified the variations in the planet survival distance induced by the stellar mass in Fig. 5, where we show the final orbit reached by the planet (a_f) versus the initial (a_o) one. This figure is more easily interpreted if compared to Fig. 1, the linear part of Fig. 5 represents the range of initial orbits that will end up at the stellar surface, the orbits that experience tidal decay but avoid engulfment are those beyond the inflection point in the figure, and finally those orbits that experience orbital expansion due to mass-loss are those that satisfy $a_f > a_o$. The different colors represent the stellar mass (see the legend at the top left corner of the plot). We have chosen for this plot stellar models with the Reimers's mass-loss prescription and the η_R=0.2 parameter. All the orbits shown in Fig. 5 have been integrated for a Jupiter mass planet.

Final values of the orbital distance larger than the initial ones imply that a planet initially located at this distance will experience an expansion of the orbit (note that the planets considered are very close to the star and unbinding is not expected; e.g. Villaver & Livio

2007). That is the case for initial orbital distances $a_o \geq 2.5\,AU$ for all the masses. Final orbital values smaller than the initial ones have two possible interpretations: (i) the planet has entered the stellar envelope and the final orbit simply reflects the value of the stellar radius (where the calculation is terminated) or (ii) the planet has suffered tidal decay reaching an orbit that avoided the stellar envelope when He-core ignition took place. These two scenarios are well separated in the plot by the inflection point in the curves. The main effect of varying the stellar mass is around the region in the plot where we find orbital decay but the planet avoids the stellar envelope. Note that for initial orbits $a_o < 2.2\,AU$ there is no difference in the final orbit induced by the stellar mass but around $2.2\,AU \leq a_o \leq 2.5\,AU$ increasing the stellar mass leads to larger final orbital distances which translates into more chances for planet survival.

A larger stellar mass decreases the influence of the mass-loss term (and its tendency to move the orbit outward) and decreases the strength of the tidal forces, effects that operate in opposite directions for planet survival (see Eq. 3). Fig. 5 shows that the stellar mass has a stronger influence through the tidal term than through the mass-loss term. This is reflected by the larger distance from the star cleared from planets (smaller color area in Fig. 5) result of the evolution of the stars with lower masses. Note also that we have chosen the least favorable scenario, the models with the smallest mass-loss rates, to show this effect. The larger the area shown beyond the inflection point the better the chances for planet survival.

3.3. Planet Mass

The dependency of the of planet survival on the RGB as a function of the planet mass using Neptunian and 1, 2, 5, and 10 M_J (Jupiter Mass) planets is shown in Fig. 6 for a 2 $M_\odot$ star with Reimers mass-loss and η_R=0.2. As already noted in VL09, for a low mass planet to be engulfed, its initial separation needs to be smaller than that of a more massive planet. This is because at equal initial separation from the star, a more massive companion exerts a stronger tidal torque (due to the dependency on q in Eq.6, 7). Note the effect of the planet's mass is negligible in the mass-loss term. Overall, survival is easier for smaller mass planets around RGB stars since they experience weaker tidal forces. Fig. 6 demonstrates that planet survival is quite sensitively dependent on the planet's mass.

Note that the case of massive companions that can tidally transfer enough angular momentum to the star and significantly spin up the primary (Garcia-Segura et al. 2014) has not been considered. In such cases, enhanced mass-loss and deformation of the primary might take place as well. Nordhaus & Spiegel (2013) estimated that this behavior starts to be important for $M_c/M_* > 0.1$, with M_c the mass of the companion, and excluded this region

of parameter space from their calculations. Note that the largest M_c/M_* we use is 6×10^{-3}, well under the Nordhaus & Spiegel (2013) estimated limit.

In Fig. 7 we show a sample of the computations to demonstrate the various effects. The left and right columns show the effect of varying the stellar mass with different planet masses, represented in the top and bottom panels of each column. Within each plot, the different mass-loss prescriptions used are shown using different colors. This figure summarizes our findings: i) that planet survival depends strongly on the planet mass and ii) that the effect of varying the planet mass dominates over changes in the mass-loss prescriptions or the stellar mass in the range considered.

The observational determination of planetary masses through the radial velocity technique carries the uncertainty of an unknown inclination angle of the orbit, and thus only minimum planet masses are available. Uncertainties in stellar masses also contribute to uncertainties in the planet mass determinations. We show that the largest uncertainties in the outcome of the process of planet survival during the RGB might be associated to the uncertainties in the planet masses and not to uncertainties in the stellar mass determination nor the mass-loss prescription used in the models.

3.4. Eccentricity Evolution

In order to consider planet's eccentricity variations we integrate equations (3–16). For the eccentricity study we have chosen two values of the mass of the planet ($1M_J, 1M_N$), two stellar masses ($1.5, 2M_\odot$), and η_R=0.5. Note that mass-loss has little effect on the planet's eccentricity, since the mass-loss rates are rather small and the orbits considered here are relatively close to the star (e.g. Veras et al. 2011). The planet's spin rate was in all cases initially 100 radians/yr but we verified that the exact initial value is unimportant.

The planet's radius was fixed at 1 Jupiter radius ($1R_J$) or $1M_N$ for the Neptune-mass planet; we did not consider the planet's radius expansion due to tidal energy being deposited in the planet's interior. The planetary tidal strength was set to $Q'_{\rm pl} = 10^5$ and the stellar properties were evolved using the models as described in §2.1 from the pre-MS. As before, the star in our models does not spin.

As noted above, for the study of the eccentricity evolution we kept the planet's radius, $R_{\rm p}$, fixed in Eqs. 10 to 12. In real systems, heating of a planet's interior by tidal forces can cause the planet to expand, further strengthening tidal forces and potentially even leading to a runaway process. This effect, important to consider in detailed studies of the evolution of MS close-in planets would have little importance for the overall outcome of the systems

considered in this paper: if they are close enough for substantial tidal heating they would be engulfed very early by the expansion of the star. Furthermore, for simplicity, we have removed from Eq. 3 the second term involving the frictional and gravitational drag forces since we have seen in the previous part of the study they have a negligible effect in reducing the semi-major axis over the RGB lifetime.

Some comments on the qualitative behavior of the effects of stellar and planetary tides are in order. The evolution the eccentricity during the MS, when the stellar radius is small, is dominated by planetary tides (e.g. Matsumura et al. 2010). During that period, the planet is rapidly brought into a state of pseudosynchronisation, where

$$\Omega_{\rm pl} = \frac{g_2}{g_5 \left(1 - e^2\right)^{3/2}} n. \tag{17}$$

Once this is attained, the planet's eccentricity decays while preserving the orbit's angular momentum, following a trajectory in the $a - e$ space

$$e = \sqrt{1 - a_f/a}. \tag{18}$$

Here, the eccentricity decays to zero as the semi-major axis decays to a finite value, a_f. In contrast, when the stellar radius is much larger, on the RGB, stellar tides dominate the evolution. Neglecting frequency dependencies for simplicity, the planet's orbit follows a trajectory,

$$e = e_0 \left(\frac{a}{a_f}\right)^{9/2}. \tag{19}$$

where e_0 is the initial eccentricity. Now the eccentricity decays to zero as the semi-major axis decays to zero. This qualitatively different behavior of the $a - e$ trajectories under stellar and planetary tides has important implications for the shape of the $a - e$ envelope, as discussed later.

In Figure 8, we show samples of the evolution of a $1 M_J$ planet on the $a - e$ plane. Evolution during the stellar MS is shown as black solid lines and on the RGB as red-dashed lines. On the MS, the planet's path is determined by planetary tides and it follows Equation 18, which brings the eccentricity down steeply while typically causing a modest decay in semi-major axis. An illustration of this path is shown in Fig. 8 as a black thick line. On the RGB, however, stellar tides dominate and the track follows a shallower path as a and e decay at similar rates (see red solid thick line). The difference in the tracks is most clearly seen in the planets starting at 0.1 AU in Fig. 8. Very distant planets do not experience tides and their orbits expand due to mass-loss. Planets at intermediate distances at around 1 AU execute a hook, as they first see their orbits expand due to mass loss but then decay tidally

as the stellar radius grows. Most of the planets plotted in Fig. 8 are eventually engulfed on the RGB.

Populations of planets in the $a - e$ plane are shown in Figure 9. To make this plot we have filled the region $a \in [0.01, 10]$ AU and $e \in [0, 0.95]$ (with e increasing in steps of 0.05) with 2964 planets and let the star and the orbit evolve. Planets with pericenters inside the stellar envelope at any time are then removed. We show the populations at meaningful times in the star's life: very early in the MS (at $\approx 20Myr$), to show the set of initial conditions being integrated, i.e. those that did not have their pericenters inside the stellar envelope during pre-MS contraction; at the start of the RGB (defined by $R_\star = 3.4R_\odot$), showing the extent of eccentricity decay during the MS, largely due to planetary tides; and at the end of the RGB, showing the clearing effects of stellar tides and the expanded stellar envelope. We included the star's pre-MS contraction phase in the calculation which limited the initial pericenters of our planet population (note we run models for the $a - e$ parameter space described above). By following the pre-MS and MS evolution the goal was not to study those phases in detail but rather to get some reasonably realistic initial conditions for the post-MS phase. Note that, while the envelope expands to only ~ 1 AU, the region out to 2-3 AU shows significant depletion of the planetary population.

Figure 10 shows the effects of varying the planetary mass on the distribution of orbital properties at the end of the RGB. As we have previously discussed we see a larger initial region of orbital distances resulting in planets getting accreted onto the stellar surface increasing as the planet mass increases. In general, we find that on the RGB, very eccentric and distant planets (a $\gtrsim$ 3 AU, e $\gtrsim$ 0.8) do not see much eccentricity decay, and their engulfment is basically just determined by their pericentre location and the maximum stellar radius.

Finally, in Figs. 11 we show how stellar tidal forces on the early RGB can create a transient population of moderately eccentric close-in Jovian planets. In Fig. 11 the envelope for *'start RGB'* is defined such that there are no planets lying above the envelope at the initial RGB output timestep. The envelope for *'all RGB'* is defined such that there are no planets lying above the envelope at any RGB output timestep, i.e. at no point on the RGB is a planet found above the envelope. For every point below the envelope, there exists at least one time, t, such that a planet is found there.

Eccentric planets with $a \lesssim 0.05$ AU are depleted on the MS due to the action of planetary tides. However, as discussed above, planetary and stellar tidal forces cause planets to follow different tracks in $a - e$ plane. Once the stellar radius begins to increase on the RGB, stellar tidal forces begin to dominate over planetary tidal forces, and the planets now follow tracks through the region depleted on the MS, with $a \sim 0.05$ AU and $e \sim 0.2$. Planets following

these tracks, however, are rapidly engulfed by the expanding stellar envelope. Neptune-mass planets do not exhibit this behavior, since the stellar tides they excite are much weaker.

4. DISCUSSION

The semi-major axis distribution of planets discovered with RV measurements radial velocity surveys as of the 1st of September 2013[1] is plotted versus the stellar mass in Fig.12. The points have been color coded according to the evolutionary status of the star, with dark blue, light blue and red representing main sequence, subgiants and red giant stars, respectively.

The planet population orbiting massive host stars (meaning M $\geq$ 1.5 $M_{\odot}$) has been claimed to be distinct with respect to the minimum orbital distances at which planets are found (see e.g., Johnson et al. 2010; Sato et al. 2008; Bowler et al. 2010). Indeed no planet around a giant has been found so far with $a < 0.54$ AU [2] (from radial velocity measurements). This fact (taken alone) has been used to suggest a relation between planet formation and the stellar mass (Currie 2009). However, as we see in Fig. 12, planets orbiting subgiant stars populate the region $a \leq 0.54$ AU and can be found as close as 0.08 AU orbiting the subgiant star HD 102956 (Johnson et al. 2010). Furthermore, recently transit surveys have discovered hot jupiters around Main Sequence A-F stars that remained elusive for radial velocity surveys (e.g. HAT-P-49 Bieryla et al. 2014; WTS-1b Cappetta et al. 2012; Kepler-14b Buchhave et al. 2011; WASP-33 Collier Cameron et al. 2010; KELT-3b Pepper et al. 2013; COGLE-TR-L9 Snellen et al. 2009). These are all mostly fairly low mass stars (1.5, 1.2, 1.5, 1.5, 1.3, and 1.5 $M_{\odot}$). The best example so far of a close-in planet around a high-mass star is HD 102956b orbiting a 1.7 $M_{\odot}$ star (Johnson et al. 2010). A transiting planet, Kepler-91b has been found at 0.072 AU from the star (Lillo-Box et al. 2013) as well, holding the record for the innermost planet found around a RGB star. Although note that the stellar mass is 1.3 $M_{\odot}$, a relatively low value compared to most RGB planet host stars, and recent claims have been made of a false positive for this system(Sliski & Kipping 2014; Esteves et al. 2013).

If close-in planets are present in the MS stage orbiting A-F stars but not found from radial velocity searches around evolved stars, this suggests that it is the evolution of the star, and not its mass, that play a role in removing planets from close orbits. In fact, as we have shown here, close-in planets enter the stellar envelope as the star leaves the main sequence

[1]Data from the exoplanet.eu, exoplanets.org (Schneider et al. 2011; Wright et al. 2011)

[2]The planets orbiting BD+15 2940 at 0.54 AU (Nowak et al. 2013), HIP 63242 at 0.57 AU (Johnson et al. 2013) hold the record.

and evolves onto the RGB (see as well Villaver & Livio 2009; Kunitomo et al. 2011). As the star evolves, it removes planets from a region that extends far beyond the stellar radius to the entire region of tidal influence ($a/R_* \approx$ 2-3; see Fig. 13 for a Jupiter mass planet). The star first, during the sub-giant phase, clears out the very close-in planets present during the MS evolution and then proceeds to clear out a larger region as the stellar radius increases when it ascends the RGB. The tidal influence region is where planets are expected to be depleted from as the star evolves. Note in Fig. 13 that most observed planets are safe from being engulfed since they are located far beyond this region. Theoretical predictions agree with the observations since there is just one planet detection with $a/R_* \leq 2.5$ (the closest one Kepler-91b has $a/R_* \approx 2.45$ Lillo-Box et al. 2013).

A feature that is harder to understand in Fig. 12 is the absence of planets in the upper middle region in the plot (no planets found around subgiant stars with $0.08 \leq a_o \leq 0.5\,AU$) and M $\geq$ 1.5 $M_\odot$. Planets are found close to massive subgiant stars, and around them beyond 0.5 AU but no subgiant with M $\geq$ 1.5 $M_\odot$ has been found with planets in that narrow range of orbits. Planets are not expected to be cleared out that far by tides during the evolution of the star along the subgiant phase. These planets are expected to be engulfed by the star later on, during the RGB evolution. So the question is, why are there planets found in the $0.08 \leq a_o \leq 0.5\,AU$ orbital range around less massive subgiants but not around subgiants with M $\geq$ 1.5 $M_\odot$?

In this paper we have explored a host mass range between 1.5 and 2 $M_\odot$ for planet survival. Within this mass range we find that during the subgiant phase planet survival is not substantially affected either by the stellar mass, or the mass-loss prescription adopted in the calculation within the reasonable assumptions adopted for the stellar models. The main parameter affecting planet survival during the subgiant phase is the planet mass. More massive planets are more likely to plunge earlier into the stellar envelope. More massive planets are formed preferentially in more massive protoplanetary disks and thus those planets are expected around more massive stars. If more massive planets are present around subgiants with M $\geq$ 1.5 $M_\odot$ then they could be brought into the stellar envelope early in the evolution if they are initially located at relatively close distance from the star and this could explain why they are not found in the $0.08 \leq a_o \leq 0.5\,AU$ orbital range. Less massive planets are harder to detect around this systems. There is an observational bias associated with the large stellar jitter in evolved hosts that prevents the detection of low mass planets around evolved stars. In fact more massive planets are found on average orbiting evolved stars (which, in principle, are more massive than the average main sequence planet hosts). The lack of observed planets around subgiants with M $\geq$ 1.5 $M_\odot$ in the $0.08 \leq a_o \leq 0.5\,AU$ orbital range is hard to understand otherwise from an theoretical perspective.

The RGB evolution is short compared to the MS lifetime, implying that the RGB region in the HR diagram is populated by stars of similar mass (for a given initial chemical composition and age). Masses for RGB (planet hosting) stars are computed from spectroscopic values of Teff and metallicities that together with visual magnitude estimates are used to interpolate in theoretical stellar evolution grids. The uncertainties involved in the measured parameters are therefore relatively large. Furthermore, the tracks for the different masses in the HR diagram are packed together and as a consequence, estimates of masses for RGB stars carry large uncertainties. Uncertainties in mass are for the most part ≤ 0.1 ($\leq 10\%$ see e.g. Maldonado et al. 2013; Mortier et al. 2013; Zieliński et al. 2012) with some objects having larger uncertainties (up to 0.3) mostly caused from the lack of available Hipparcos parallaxes van Leeuwen (2007). The stellar radius have the same dominant source for the uncertainty as the stellar mass and have values of $\approx$ 6–15 %. We have shown that mass differences within the studies range do not have a strong influence on planet survival along the RGB and thus mass observed mass uncertainties should not have a strong influence in the outcome of the distribution of observed planets.

It has been argued that the planet survival limit is rather sensitive to the host's star mass (Kunitomo et al. 2011). While this is true when the stellar mass crosses from low to intermediate mass (where the stellar core conditions change from degenerate to not degenerate), it is not true when low mass stars are involved. Along these lines it is important to remember that while the RGB T_{eff} at a given luminosity is only slightly sensitive to the value of the stellar mass, it is affected by the initial value of the metallicity Z. Increasing Z moves the transition between low and intermediate mass stars towards higher masses. Higher mass stars would ascend the RGB faster and grow smaller in radius (note that this transition mass is set al 1.4 $M_{\odot}$ in Lloyd (2013) where he argues for lower mass planet hosting evolved stars than claimed in the literature). Our limit for He-flash stars is at 2.5 $M_{\odot}$ for [Fe/H]= 0.19. It is the mass limit between degenerate and non-degenerate cores that strongly influences the planet survival limit during the RGB. Close-in planets thus would have more chances to survive orbiting metal poor stars due to this effect. Note the mass limit to build a degenerate core during the RGB is 1.5 $M_{\odot}$ for Z=0.01 $Z_{\odot}$ (Sweigart et al. 1990).

We have shown that for a given mass-loss prescription, increasing the stellar mass puts more planets into the safe zone limit. This is because the stellar mass has a stronger influence (through the tidal term) than the mass-loss term.

In Fig. 14 we show the distribution of stellar radi as a function of orbital separation for planets found in radial velocity surveys. The planets clearly occupy different regions according to the evolutionary status of the star. In this plot, the striking feature is the lack

of planetary systems found orbiting giant stars at large distances, beyond 3 AU. There is nothing in principle that could cause this region to be depleted of planets unless stellar jitter is preventing the detection at large distances or planet searches around giant stars have not been carried long enough to recover this planet population present, on the other hand around MS stars. We find that all the observed systems are within the a/R_* safe zone from tidal interaction we find from the calculation of the orbital evolution.

Regarding the eccentricities of planet orbits, the observed distribution is shown in Fig. 15. According to theoretical expectations giant stars being systems dominated by stellar tides tend to have a and e decaying at similar rates. It is expected therefore that planets experiencing tidal eccentricity decay would as well experience orbital decay and thus would not be observed. Subgiants and MS stars on the other hand, could have experienced eccentricity decay but not substantial orbital decay, explaining the upper left corner clearance zone in the plot.

In summary, our calculations show that rapid tidal orbital decay occurs when $a/R_* <3$. There are only 3 planets found orbiting RGB stars with $a/R_* <10$, and none has been found with $a/R_* <8$. The region $\in[0.08,\ 0.5]$ AU around subgiants is too wide to have been depleted of planets just by tidal effects, so the depletion must have other origins and cannot be primordial since this planets have been found recently orbiting A-F MS stars using imaging techniques. A mass dependent mechanism must be at play that can only act in one way by building more massive planets are around more massive hosts that due to tidal forces are brought into the stellar envelope from larger initial orbital distances. The only way that makes sense is if the RGB stars are indeed higher mass, distinct from the MS planet hosts. If the RGB stars are low mass, as Lloyd (2013) and Schlaufman & Winn (2013) argue, then there is no sensible way of accounting for the lack of close-in RGB planets since the stellar radius is too small to cause depletion by tidal forces (unless the stellar radii are systematically underestimated, by a factor of 3 or more).

5. CONCLUSIONS

In this work we have quantified the influence of different parameters on the survival of planets orbiting subgiant and red giant stars. We have explored a mass range for the hosts between 1.5 and 2 $M_\odot$ and find that during the subgiant phase planet survival is not substantially affected either by the stellar mass, or the adopted mass-loss prescription. The main parameter affecting planet survival during the subgiant phase is the planet mass, with more massive planets being more likely to plunge earlier into the stellar envelope.

We find that even though the observed uncertainties in the determination of the stellar mass or mass-loss rates are quite large, those do not have much influence on the critical orbit beyond which a planet will survive RGB evolution. Since tidal torques drop as a high negative power of the ratio of stellar radius to orbital separation, companions that escape engulfment experience essentially no tidal interactions if they are located beyond a certain initial orbit. Planets located at $a/R_* \approx$ 2-3 are in jeopardy as soon as the star leaves the MS since that is where the tidal force starts to dominate the orbital evolution.

Eccentric planets with $a \lesssim 0.05$ AU are depleted on the MS due to the action of planetary tides. However, once the stellar radius begins to increase on the RGB, stellar tidal forces begin to dominate over planetary tidal forces, and planets follow tracks through the region depleted on the MS, with $a \sim 0.05$ AU and $e \sim 0.2$. Planets following these tracks, however, are rapidly swallowed by the expanding stellar envelope. Also important is that we find that during the RGB very eccentric and distant planets do not experience much eccentricity decay, and that planet engulfment is basically just determined by pericentre location and the maximum stellar radius.

E.V. and A. J. M.'s work was supported by the Spanish Ministerio de Ciencia e Innovación (MICINN), Plan Nacional de Astronomía y Astrofísica, under grant AYA2010-20630 and by the Marie Curie program under grant FP7-People-RG268111. LS is a FNRS research associate. We thank Amy Bonsor for useful discussions

REFERENCES

Adams, F. C., & Bloch, A. M. 2013, ApJ, 777, L30

Alexander, M. E., Chau, W. Y., & Henriksen, R. N. 1976, ApJ, 204, 879

Bear, E., & Soker, N. 2011, MNRAS, 411, 1792

Bieryla, A., Hartman, J. D., Bakos, G. A., et al. 2014, arXiv:1401.5460

Bowler, B. P., Johnson, J. A., Marcy, G. W., et al. 2010, ApJ, 709, 396

Buchhave, L. A., Latham, D. W., Carter, J. A., et al. 2011, ApJS, 197, 3

Carlberg, J. K., Majewski, S. R., & Arras, P. 2009, ApJ, 700, 832

Carlberg, J. K., Majewski, S. R., Patterson, R. J., et al. 2011, ApJ, 732, 39

Cappetta, M., Saglia, R. P., Birkby, J. L., et al. 2012, MNRAS, 427, 1877

Charpinet, S., Fontaine, G., Brassard, P., et al. 2011, Nature, 480, 496

Collier Cameron, A., Guenther, E., Smalley, B., et al. 2010, MNRAS, 407, 507

Currie, T. 2009, ApJ, 694, L171

Debes, J. H., & Sigurdsson, S. 2002, ApJ, 572, 556

de Medeiros, J. R., Da Rocha, C., & Mayor, M. 1996, A&A, 314, 499

Dobbs-Dixon, I., Lin, D. N. C., & Mardling, R. A. 2004, ApJ, 610, 464

Duncan, M. J., & Lissauer, J. J. 1998, Icarus, 134, 303

Esteves, L. J., De Mooij, E. J. W., & Jayawardhana, R. 2013, ApJ, 772, 51

Garcia-Segura, G., Villaver, E., Langer, N., Yoon, S.-C., & Manchado, A. 2014, arXiv:1401.4414

Grevesse N., Noels A., Sauval A.J. 1996, ASPC, 99, 117

Goldreich, P., & Nicholson, P. D. 1977, Icarus, 30, 301

Iben, I., Jr. 1967, ARA&A, 5, 571

Jackson, B., Greenberg, R., & Barnes, R. 2008, ApJ, 678, 1396

Jackson, B., Greenberg, R., & Barnes, R. 2008, ApJ, 681, 1631

Jackson, B., Barnes, R., & Greenberg, R. 2009, ApJ, 698, 1357

Johnson, J. A., et al. 2007, ApJ, 670, 833

Johnson, J. A., Bowler, B. P., Howard, A. W., et al. 2010, ApJ, 721, L153

Johnson, J. A., Morton, T. D., & Wright, J. T. 2013, ApJ, 763, 53

Jones, M. I., Jenkins, J. S., Rojo, P., Melo, C. H. F., & Bluhm, P. 2013, A&A, 556, A78

Kratter, K. M., & Perets, H. B. 2012, ApJ, 753, 91

Kunitomo, M., Ikoma, M., Sato, B., Katsuta, Y., & Ida, S. 2011, ApJ, 737, 66

Lillo-Box, J., Barrado, D., Moya, A., et al. 2013, arXiv:1312.3943

Livio, M. & Soker, N. 1984, MNRAS, 208, 763

Livio, M., & Soker, N. 1988, ApJ, 329, 764

Lloyd, J. P. 2013, ApJ, 774, L2

Lovis, C. & Mayor, M. 2007, A&A, 472, 657

Maldonado, J., Villaver, E., & Eiroa, C. 2013, A&A, 554, A84

Massarotti, A., Latham, D. W., Stefanik, R. P., & Fogel, J. 2008, AJ, 135, 209

Matsumura, S., Peale, S. J., & Rasio, F. A. 2010, ApJ, 725, 1995

Moeckel, N., & Veras, D. 2012, MNRAS, 422, 831

Mortier, A., Santos, N. C., Sousa, S. G., et al. 2013, A&A, 557, A70

Mustill, A. J., & Villaver, E. 2012, ApJ, 761, 121

Niedzielski, A., Goździewski, K., Wolszczan, A., et al. 2009, ApJ, 693, 276

Nordhaus, J., & Blackman, E. G. 2006, MNRAS, 370, 2004

Nordhaus, J., Spiegel, D. S., Ibgui, L., Goodman, J., & Burrows, A. 2010, MNRAS, 408, 631

Nordhaus, J., & Spiegel, D. S. 2013, MNRAS, 432, 500

Nowak, G., Niedzielski, A., Wolszczan, A., Adamów, M., & Maciejewski, G. 2013, ApJ, 770, 53

Ogilvie, G. I., & Lesur, G. 2012, MNRAS, 422, 1975

Ogilvie, G. I. 2014, arXiv:1406.2207

Ostriker, E. C. 1999, ApJ, 513, 252

Passy, J.-C., Mac Low, M.-M., & De Marco, O. 2012, ApJ, 759, L30

Penev, K., Sasselov, D., Robinson, F., & Demarque, P. 2007, ApJ, 655, 1166

Penev, K., & Sasselov, D. 2011, ApJ, 731, 67

Pepper, J., Siverd, R. J., Beatty, T. G., et al. 2013, ApJ, 773, 64

Rasio, F. A., Tout, C. A., Lubow, S. H., & Livio, M. 1996, ApJ, 470, 1187

Reffert, S., Quirrenbach, A., Mitchell, D. S., Albrecht, S., Hekker, S., Fischer, D. A., Marcy, G. W., & Butler, R. P. 2006, ApJ, 652, 661

Reimers, D. 1975, Men. Soc. Roy. Sci. Liége, 6th Ser. 8, 369

Rosenhead, L. (ed.) 1963, *Laminar Boundary Layer* (Oxford: Clarendon Press)

Sato, B., et al. 2007, ApJ, 661, 527

Sato, B., et al. 2008, PASJ, 60, 539

Schröder, K.-P., & Cuntz, M. 2005, ApJ, 630, L73

Siess, L. 2006, A&A, 448, 717

Siess, L. & Livio, M. 1999a, MNRAS, 304, 925

Siess, L. & Livio, M. 1999b, MNRAS, 308, 1133

Snellen, I. A. G., Koppenhoefer, J., van der Burg, R. F. J., et al. 2009, A&A, 497, 545

Schlaufman, K. C., & Winn, J. N. 2013, ApJ, 772, 143

Schneider, J., Dedieu, C., Le Sidaner, P., Savalle, R., & Zolotukhin, I. 2011, A&A, 532, A79

Sliski, D. H., & Kipping, D. M. 2014, arXiv:1401.1207

Sweigart, A. V., Greggio, L., & Renzini, A. 1989, ApJS, 69, 911

Sweigart, A. V., Greggio, L., & Renzini, A. 1990, ApJ, 364, 527

van Leeuwen, F. 2007, A&A, 474, 653

Veras, D., Wyatt, M. C., Mustill, A. J., Bonsor, A., & Eldridge, J. J. 2011, MNRAS, 417, 2104

Veras, D., Mustill, A. J., Bonsor, A., & Wyatt, M. C. 2013, MNRAS, 431, 1686

Verbunt, F. & Phinney, E. S. 1995, A&A, 296, 709

Villaver, E. & Livio, M. 2007, ApJ, 661, 1192

Villaver, E., & Livio, M. 2009, ApJ, 705, L81

Witte, M. G., & Savonije, G. J. 2002, A&A, 386, 222

Wright, J. T., Upadhyay, S., Marcy, G. W., Fischer, D. A., Ford, E. B., & Johnson, J. A. 2009, ApJ, 693, 1084

Wright, J. T., Fakhouri, O., Marcy, G. W., et al. 2011, PASP, 123, 412

Zahn, J. P. 1966, Annales d'Astrophysique, 29, 489

Zahn, J.-P. 1977, A&A, 57, 383

Zahn, J.-P. 1989, A&A, 220, 112

Zieliński, P., Niedzielski, A., Wolszczan, A., Adamów, M., & Nowak, G. 2012, A&A, 547, A91

This preprint was prepared with the AAS LaTeX macros v5.2.

$M_{\rm ini}$ $[M_\odot]$	wind	$M_{\rm 1DUP}$ $[M_\odot]$	$M_{\rm tip}$ $[M_\odot]$	$R_{\rm tip}$ $[R_\odot]$	$L_{\rm tip}$ $[L_\odot]$	$M_{\rm tip}^{\rm core}$ $[M_\odot]$	$\dot{M}_{\rm tip}$ $[M_\odot/{\rm yr}]$	$t_{\rm RGB}$ [Myr]	a_c, $M_p = M_J$ [AU]
1.5	$\eta_R = 0.2$	1.497	1.410	216.2	3015.4	0.489	3.469×10^{-8}	203.9	2.43
1.5	$\eta_R = 0.5$	1.494	1.304	196.4	2560.4	0.472	7.251×10^{-8}	203.6	2.11
1.5	$\eta_R = 0.5$+OS	1.494	1.272	221.9	2913.2	0.485	9.465×10^{-8}	197.5	2.10
1.5	Sc	1.490	1.369	190.3	2547.7	0.471	6.834×10^{-8}	206.3	2.14
1.6	$\eta_R = 0.2$	1.597	1.516	209.2	3027.7	0.490	3.152×10^{-8}	185.1	2.38
1.6	$\eta_R = 0.5$	1.594	1.393	209.4	2871.6	0.483	8.105×10^{-8}	186.6	2.20
1.6	Sc	1.589	1.448	209.4	2960.1	0.486	8.924×10^{-8}	190.1	2.04
1.7	$\eta_R = 0.2$	1.697	1.620	204.8	3072.7	0.491	2.946×10^{-8}	190.2	2.34
1.7	$\eta_R = 0.5$	1.694	1.519	191.2	2705.1	0.477	6.458×10^{-8}	190.3	2.09
1.7	$\eta_R = 0.5$+OS	1.694	1.509	201.8	2888.1	0.484	7.300×10^{-8}	154.2	2.07
1.7	Sc	1.688	1.590	176.8	2542.8	0.470	4.904×10^{-8}	176.7	2.03
1.8	$\eta_R = 0.2$	1.797	1.724	202.2	3128.0	0.493	2.791×10^{-8}	161.5	2.29
1.8	$\eta_R = 0.5$	1.794	1.638	177.1	2569.4	0.472	5.300×10^{-8}	162.5	1.99
1.8	Sc	1.787	1.686	181.9	2716.6	0.477	5.108×10^{-8}	183.9	2.09
1.9	$\eta_R = 0.2$	1.898	1.827	198.2	3155.4	0.493	2.613×10^{-8}	149.9	2.25
1.9	$\eta_R = 0.5$	1.894	1.727	190.1	2898.6	0.484	6.082×10^{-8}	149.3	2.09
1.9	$\eta_R = 0.5$+OS	1.894	1.732	191.0	2934.7	0.486	6.170×10^{-8}	86.9	2.09
1.9	Sc	1.885	1.786	184.2	2847.2	0.481	5.091×10^{-8}	146.1	2.09
2.0	$\eta_R = 0.2$	1.997	1.930	193.9	3166.5	0.494	2.434×10^{-8}	148.7	2.21
2.0	$\eta_R = 0.5$	1.995	1.821	198.6	3155.7	0.494	6.560×10^{-8}	145.9	2.15
2.0	Sc	1.984	1.874	196.0	3173.7	0.494	6.032×10^{-8}	160.2	2.19

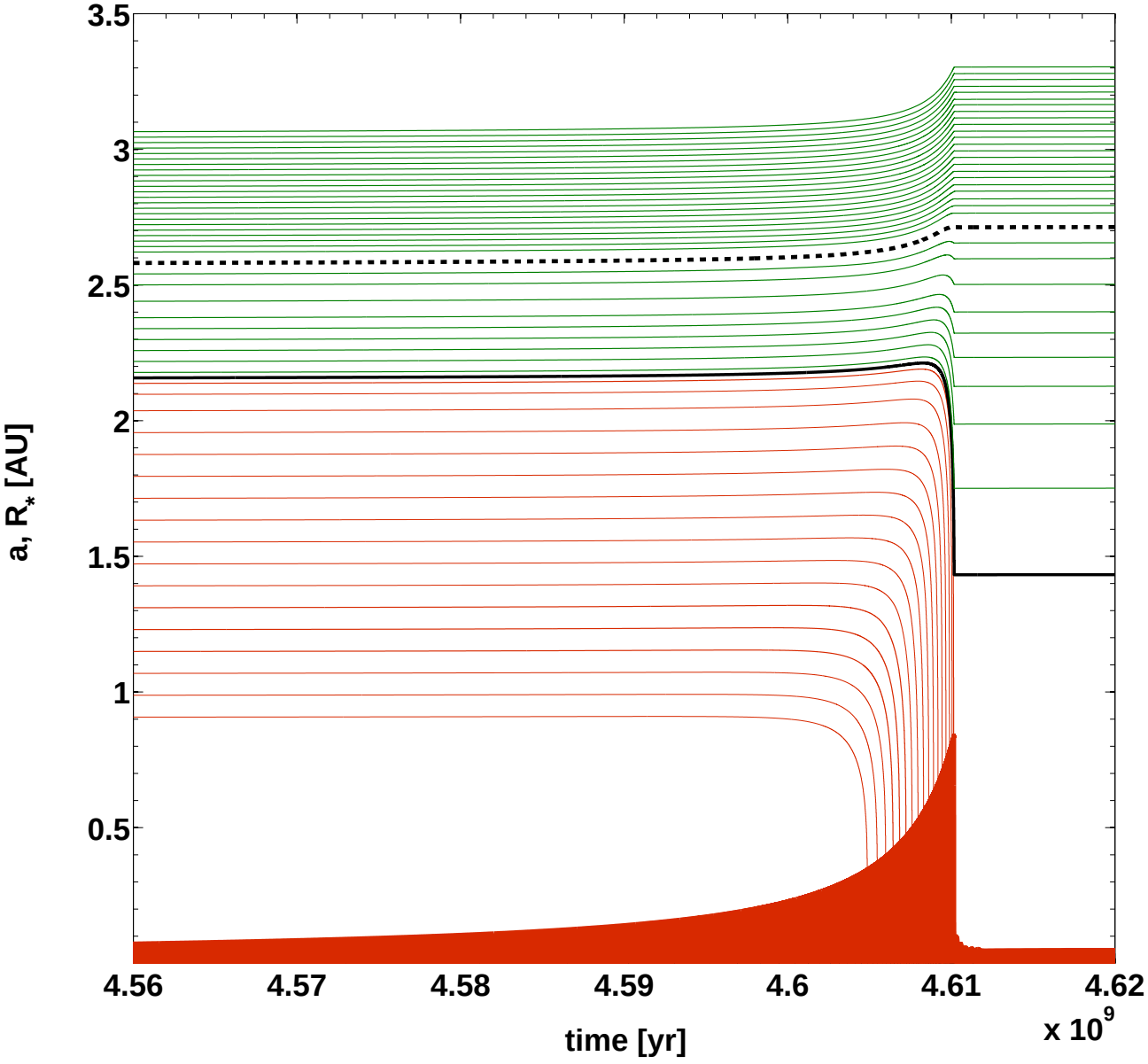

Fig. 1.— The filled red area represents 0.06 Gyr in the evolution of the stellar radius as the star goes to the tip of the RGB. The star has a mass of 1.5 $M_{\odot}$ and is evolving under the Schröder & Cuntz(2005) mass-loss prescription. The evolution of a set of orbits of a planet with 1 Jupiter mass is shown as well, with the red lines representing a set of initial separations for which the planet ends up inside the stellar envelope. The green lines represent the initial separations for which the planet avoids engulfment. The solid black line is the minimum initial orbit for which the planet avoids being engulfed and the dashed black line marks the initial orbit beyond which the planet is not affected by the tidal forces.

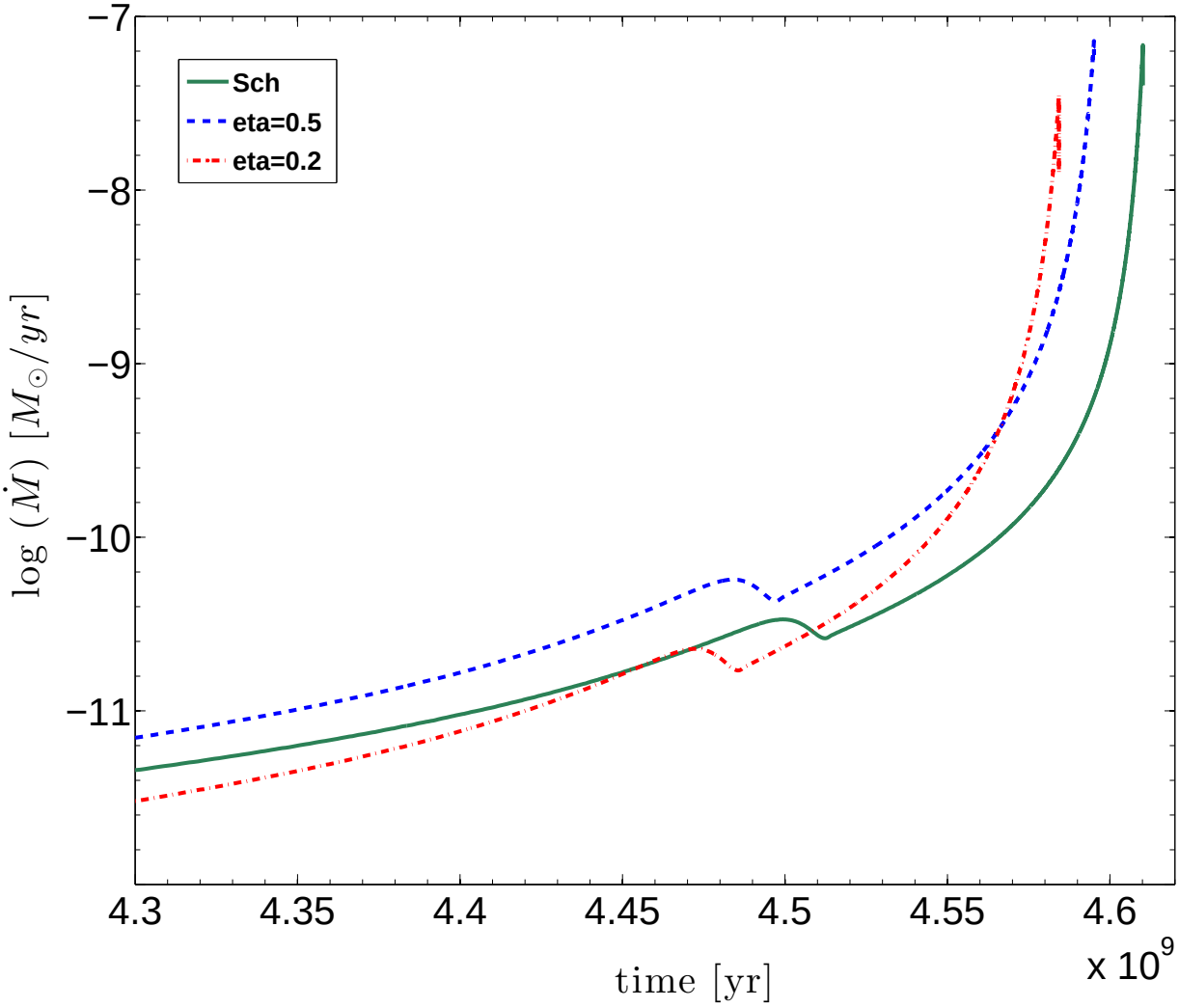

Fig. 2.— Mass-loss rates for 1.5 $M_{\odot}$ stars during the last years of the RGB evolution under $\eta_R = 0.2$ (red dot-dashed), $\eta_R = 0.5$ (blue dashed), and Schröder & Cuntz (2005) (green solid line).

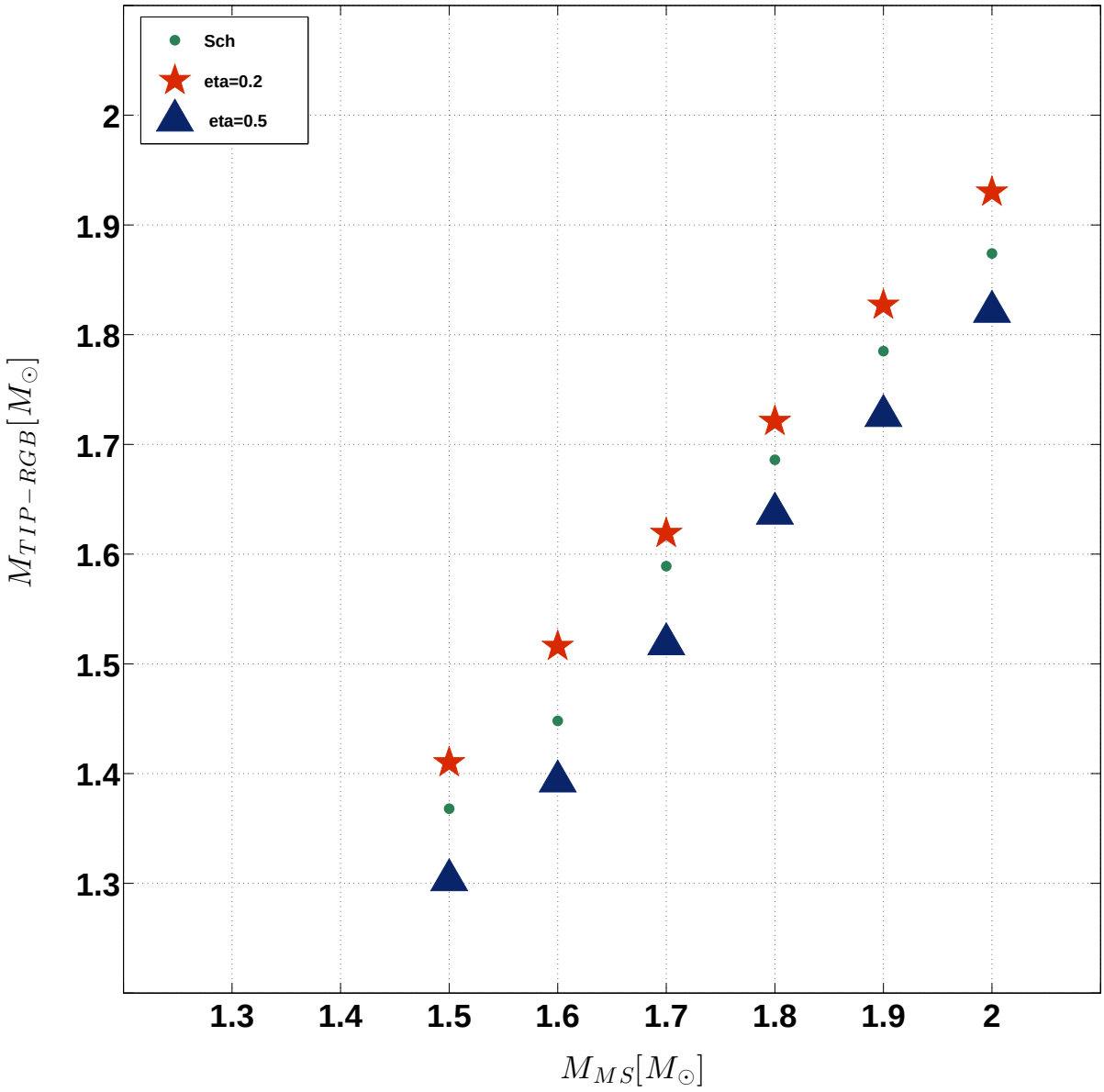

Fig. 3.— Mass of the star at the tip of the RGB in solar units versus the MS mass of the star. The different symbols correspond to the 3 prescriptions used and are indicated in the legend (red stars ($\eta_R = 0.2$), blue triangles ($\eta_R = 0.5$), and green asterisks(Schröder & Cuntz 2005).

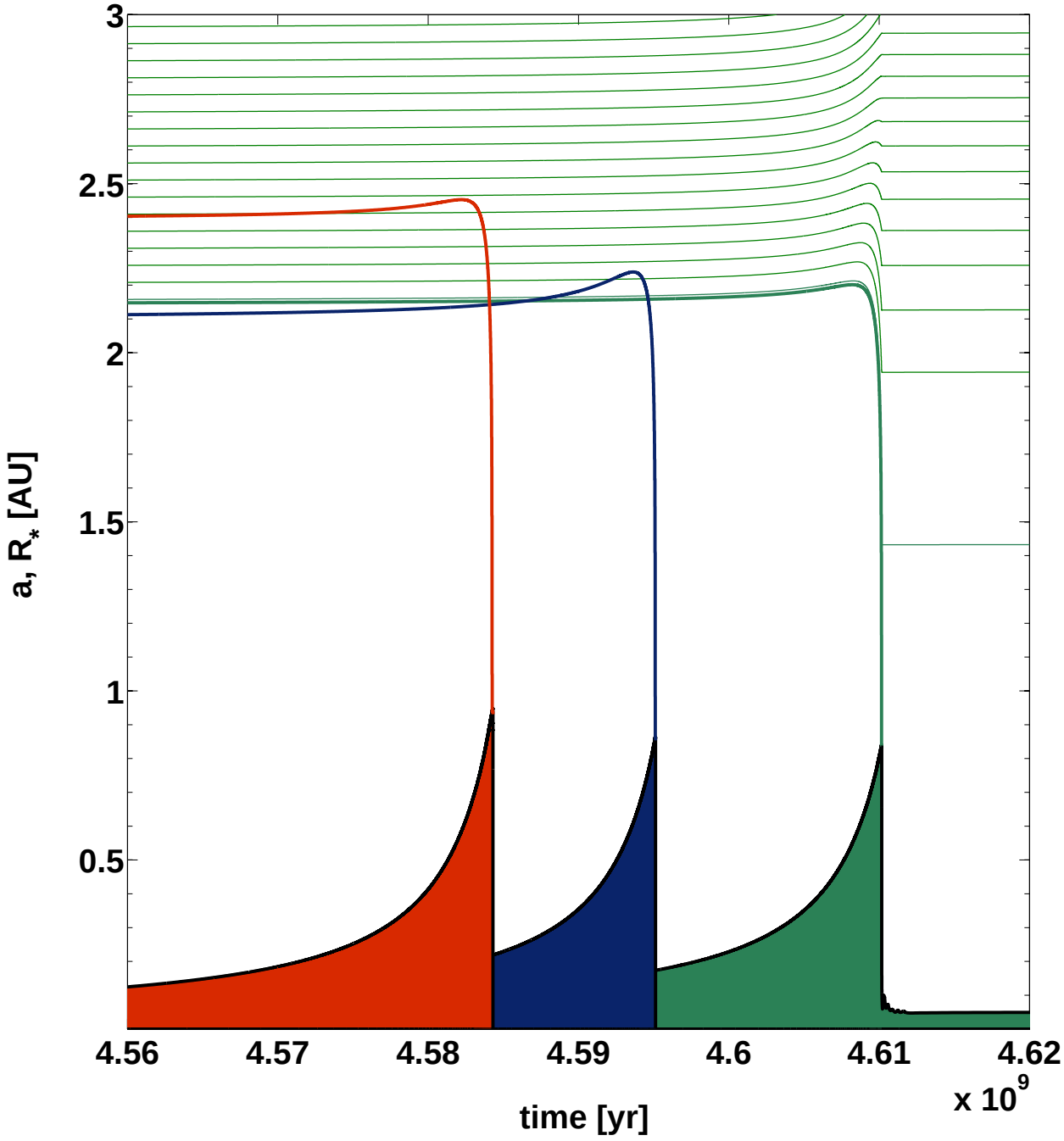

Fig. 4.— The red ($\eta_R = 0.2$), blue ($\eta_R = 0.5$), and green (Schröder & Cuntz 2005) areas represent the evolution of the stellar radius of a 1.5 $M_\odot$ to the RGB tip. The solid lines are the maximum initial orbital radius for which the planet gets engulfed and are color coded according to the stellar model. For the Schröder & Cuntz (2005) mass-loss prescription model (green) a set of orbits that avoid engulfment are shown.

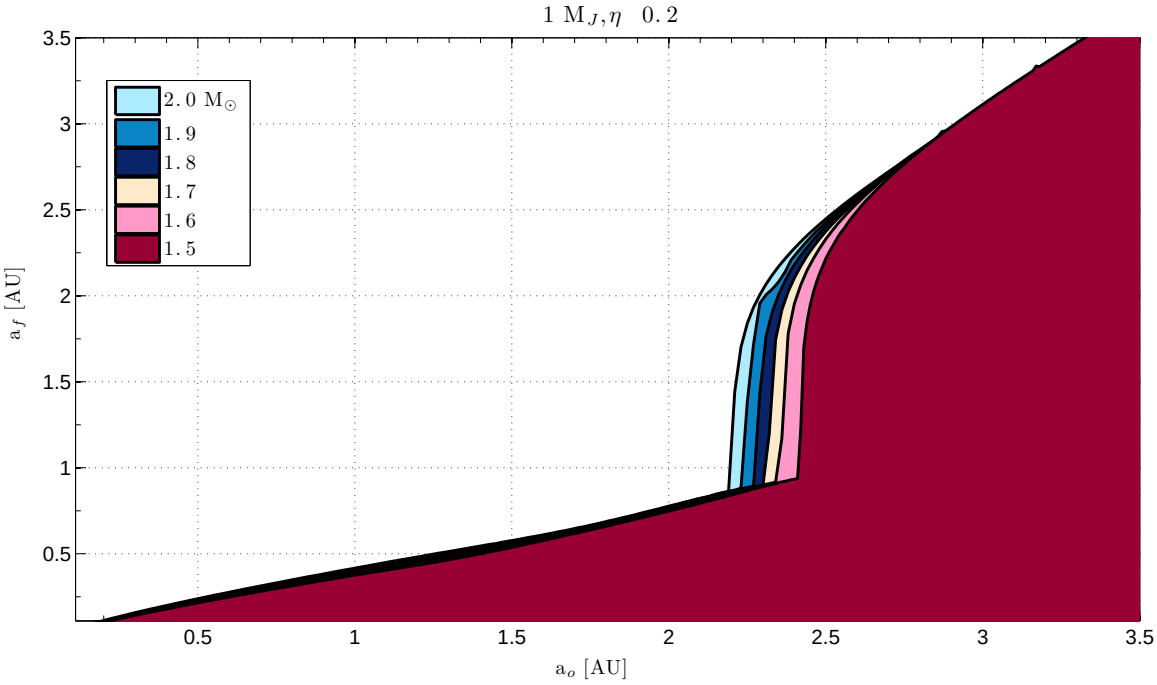

Fig. 5.— Final (a_f) versus initial (a_o) orbit reached by a planet of a Jupiter mass at the end of the RGB for stellar models with masses between 1.5 and 2 $M_\odot$. The mass-loss prescription adopted for the models shown is that of Reimers with $\eta_R = 0.2$. The different area colors represent the different stellar masses as indicated in the legend shown in the upper left corner. Planets with final orbits equal or larger than the initial ones survive the RGB evolution of the star. Planets with initial orbits smaller than that at the inflexion point in the curves are engulfed by the stellar envelope. Planets with initial orbits in the narrow range between the inflexion point and the 1:1 relation experienced tidal decay but remain outside the stellar envelope as the latter contracted following He core ignition.

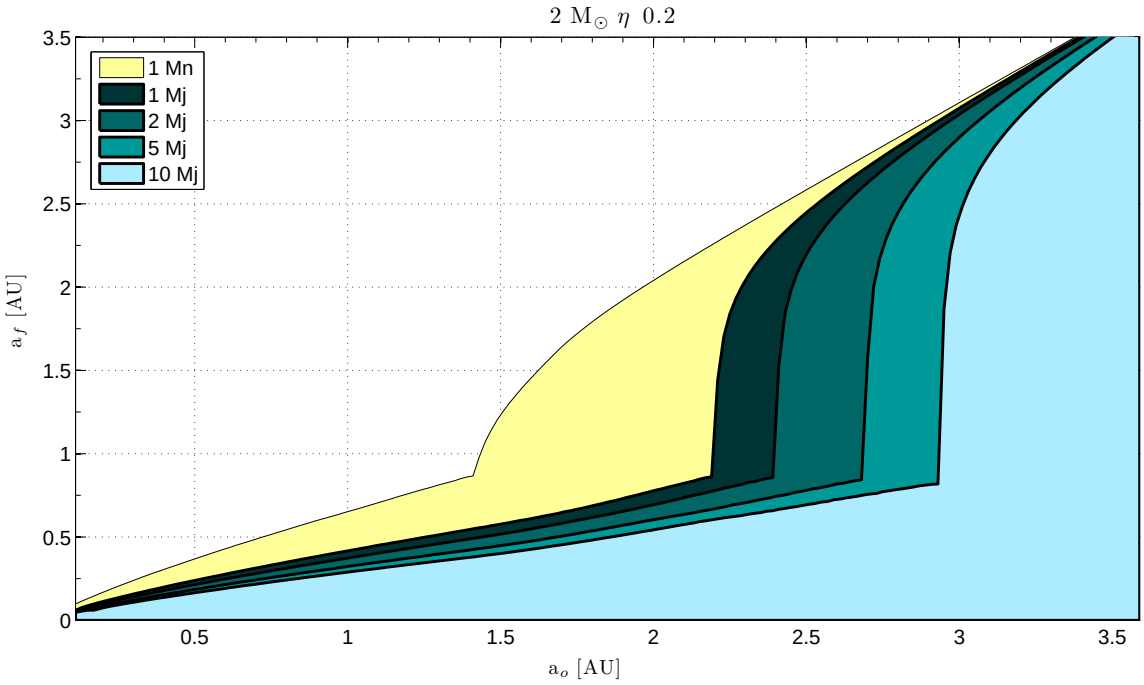

Fig. 6.— Same as Fig. 5 but using a star with 2 $M_\odot$, Reimers mass-loss with $\eta_R = 0.2$, and varying the planet mass between Neptune mass ($1M_N$ in the legend in the top left corner) and 1, 2, 5 and 10 Jovian masses (10 M_J light blue area).

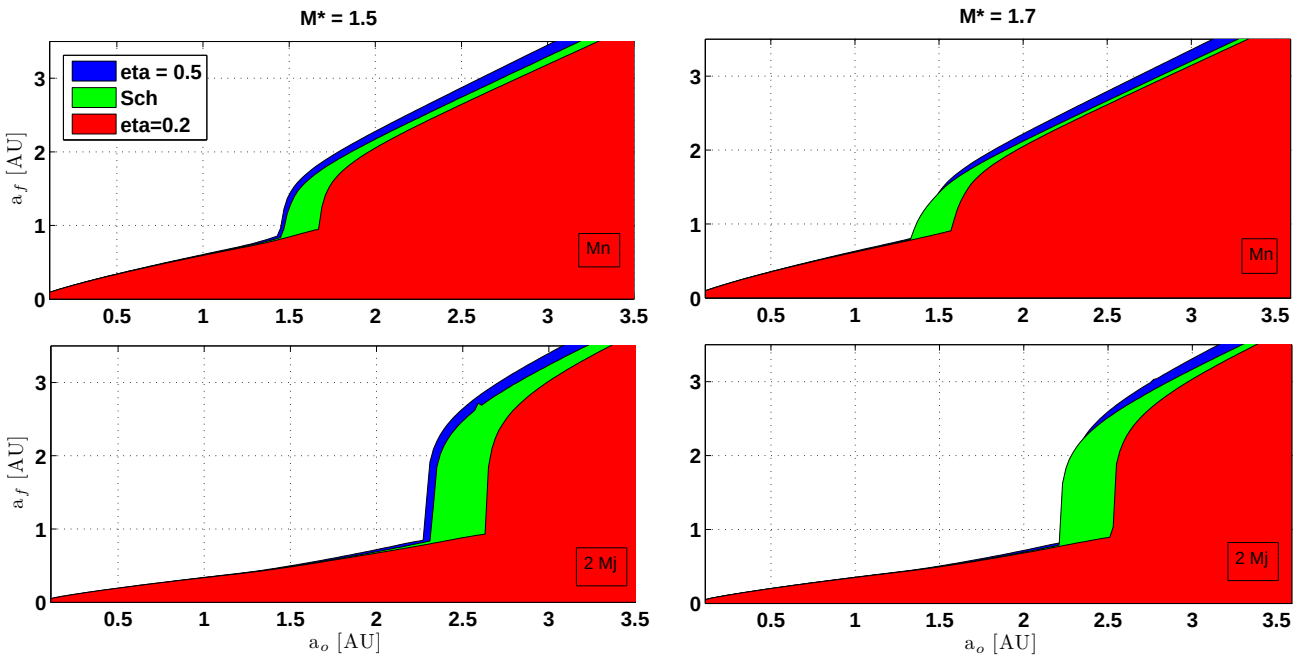

Fig. 7.— Left column, variation under the mass-loss prescriptions used in the stellar evolution calculations of the final (a_f) versus initial (a_o) orbit of a planet orbiting a 1.5 $M_\odot$ star. The top panels are for a planet with Neptune mass and the bottom plots are for planets with twice the mass of Jupiter. Right column, the same but for a star with 1.7 $M_\odot$. The legend at the top left corner gives the mass-loss prescriptions used in the calculation of the stellar structure. The mass of the star is indicated at the top of each column and the planet mass at the bottom right corner of each plot.

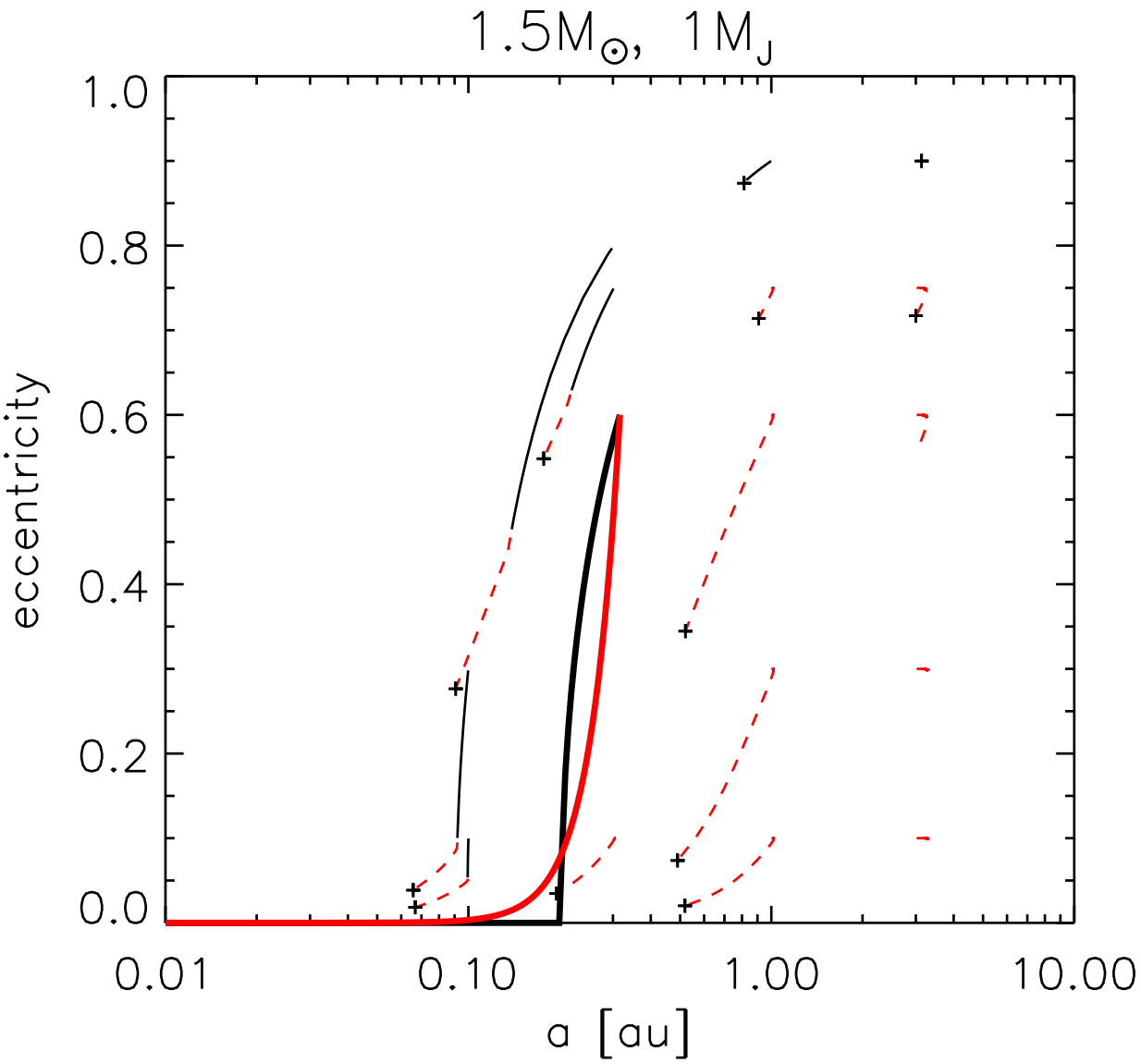

Fig. 8.— Sample evolutionary tracks in $a-e$ space of planets of mass $1\,M_J$ orbiting a $1.5\,M_\odot$ star. Linestyles show different evolutionary phases: solid black line MS and dashed line the RGB. Crosses indicate where planets are engulfed by the star. The solid and red thick lines show the analytical approximation for the evolution on the MS and RGB respectively (Eqs. 16 and 17).

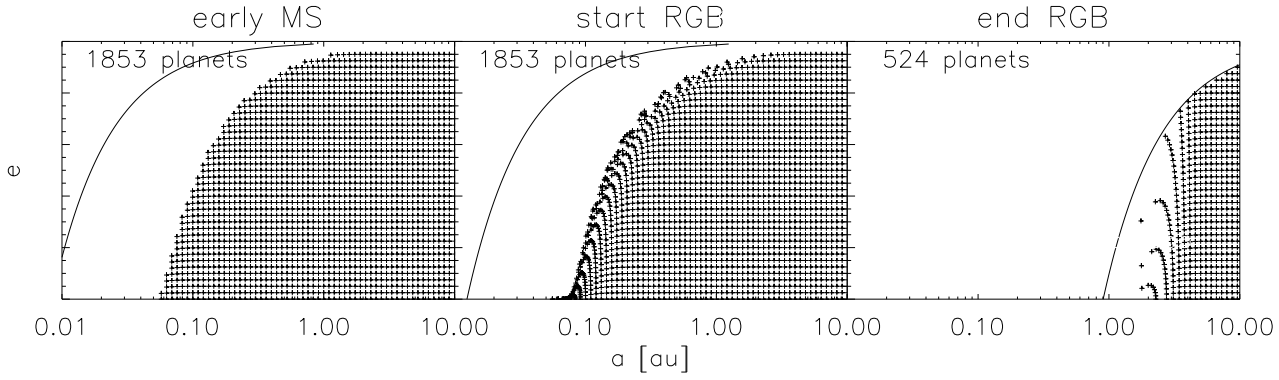

Fig. 9.— Populations of $1M_J$ planets orbiting $1.5M_\odot$ stars at three points in the star's life: early MS (left) $\approx$ 20 Myr, beginning of RGB (center), and end of RGB (right). The solid line marks the locus where the planets' pericenters lie on the stellar surface. The number of planets is shown in each panel

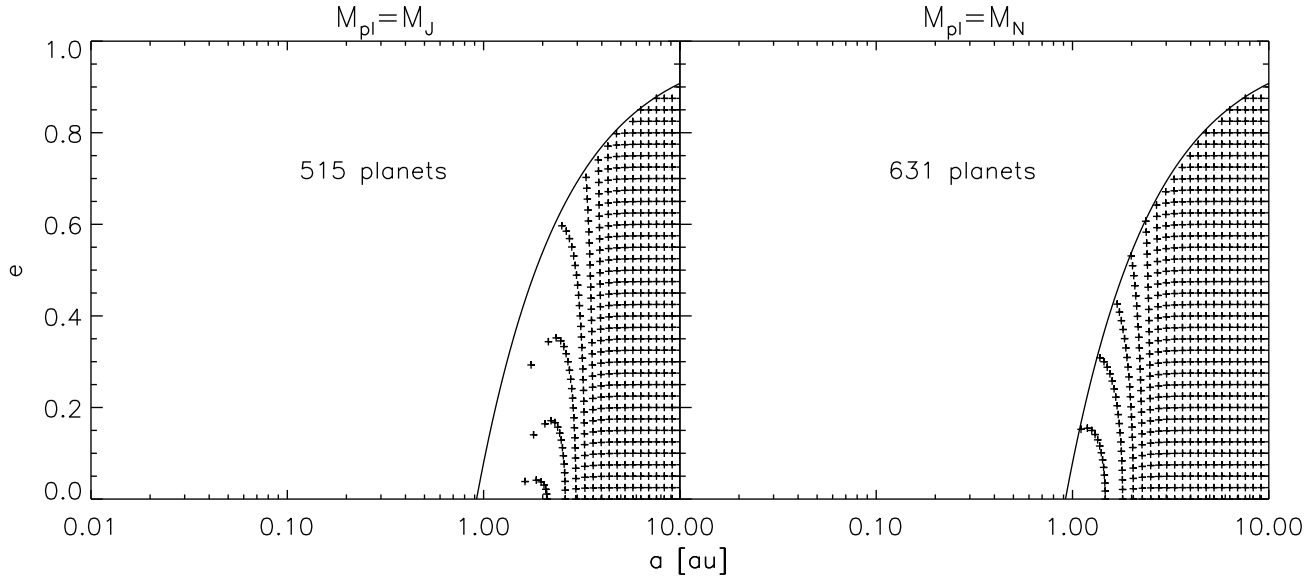

Fig. 10.— The effects of changing the planet mass on the planet population surviving the RGB. Left to right: $2M_\odot$ and $1M_J$; $2M_\odot$ and $1M_N$.

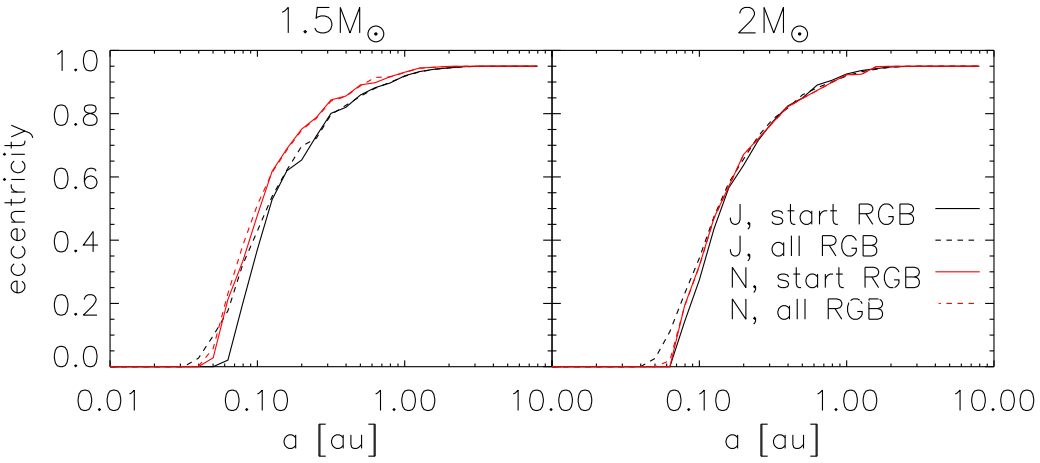

Fig. 11.— Envelopes of planet populations around $1.5M_\odot$ and $2M_\odot$ stars (left and right panels respectively). Envelopes of the population at the beginning of the RGB are shown as solid lines, while envelopes over the *whole* RGB population are shown as dashed lines. Stellar tides cause some Jovian planets to decay through a region of moderate eccentricity and small semi-major axis that was depleted during MS evolution by planetary tides.

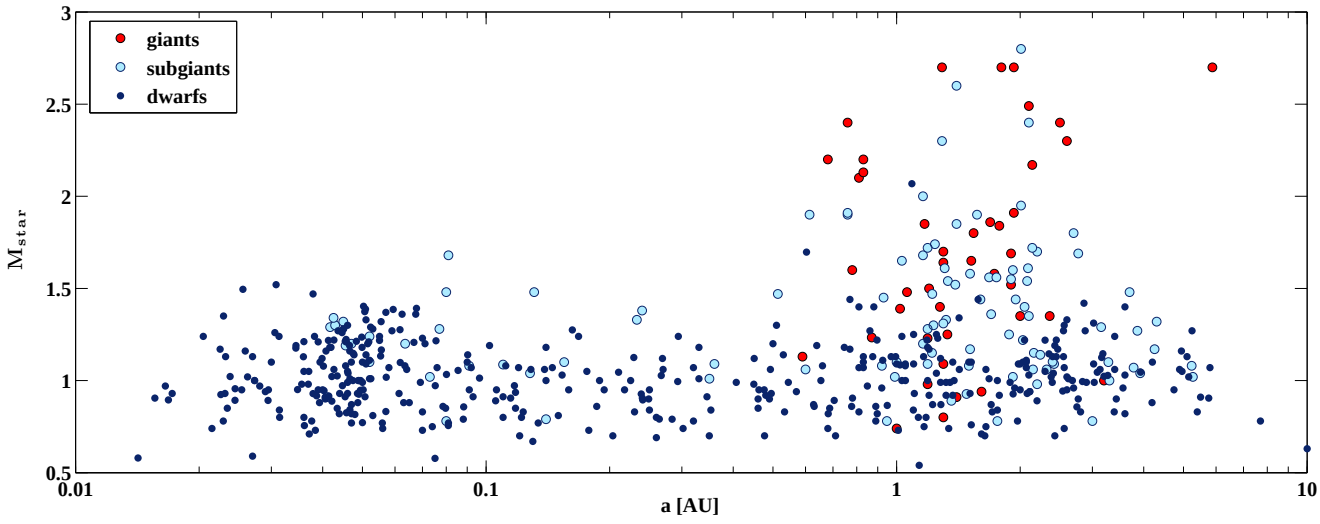

Fig. 12.— The observed orbital distance versus the stellar mass of all the confirmed planets detected through the radial velocity method taken from the Exoplanet encyclopedia (exoplanet.eu, exoplanets.org). The different colors represent the evolutionary status of the star as determined by the published luminosity class.

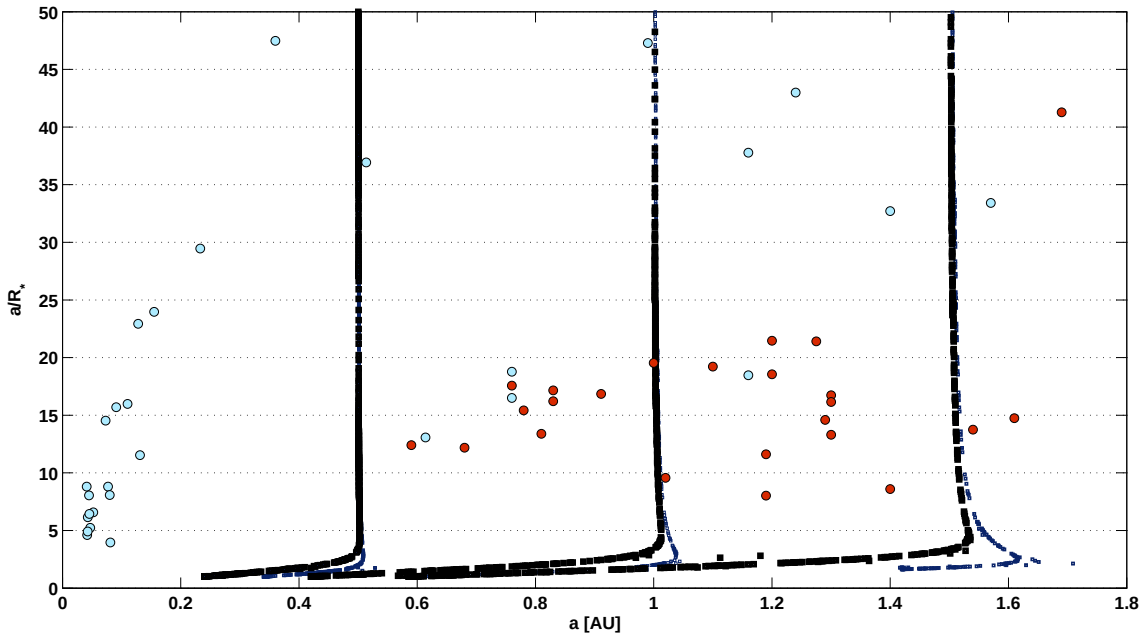

Fig. 13.— Ratio of the orbital distance to the stellar radius versus the orbital distance of the observed population of planets orbiting subgiant stars (light blue points) and giant stars (red points). The evolution of the orbital to stellar ratio is shown for 3 initial orbital distance (0.5, 1 and 1.5 AU) and two stellar masses 1.5 $M_{\odot}$ (in dark blue) and 2 $M_{\odot}$ (in black) and for a jupiter mass planet.

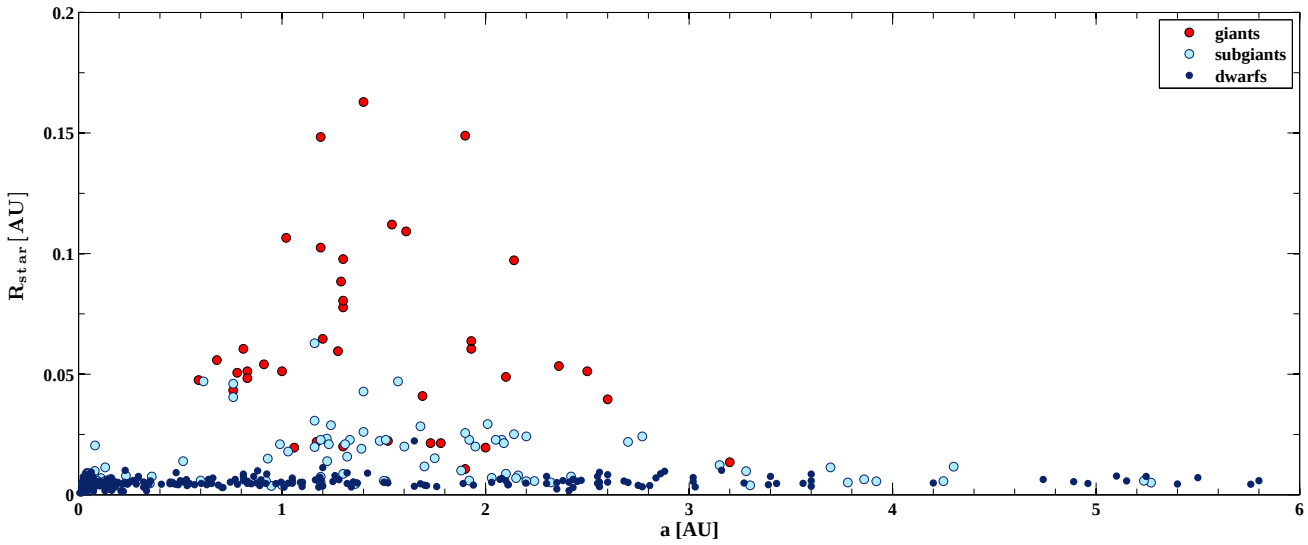

Fig. 14.— Same as Fig. 12 but here the observed orbital distance is plotted against the stellar radius.

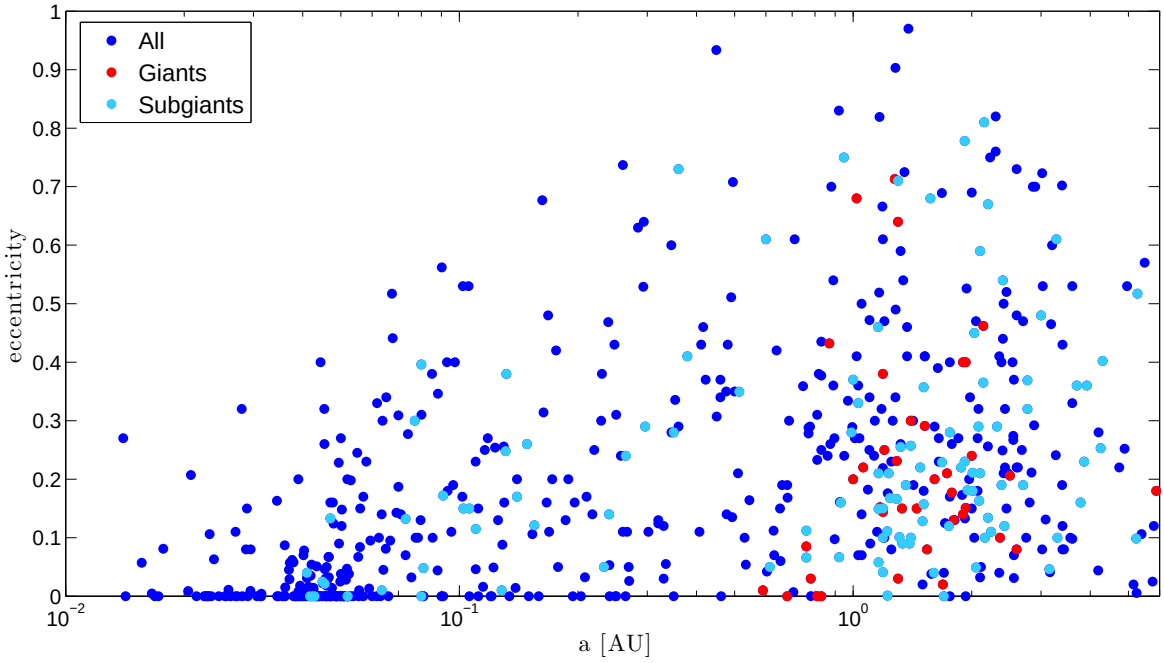

Fig. 15.— Same as Fig. 12 but here the observed planet eccentricity is plotted versus orbital distance.